

CHAPTER 5

FLOW PATTERNS AND WALL SHEAR STRESS IN ARTERIES

III BRANCHED TUBES AND FLOW INSTABILITY

5.1 Flow in symmetric bifurcations

Most branchings in the cardiovascular system are asymmetric, the only major exception in man being the bifurcation where the aorta divides to form the iliac arteries. This is in contrast to the bifurcating airways of the lung, for which the assumption of symmetry is more appropriate, and which have been the subject of extensive research (Pedley, 1977). Furthermore, the precise definition of an asymmetric bifurcation requires the specification of several more parameters than that of a symmetric one (e.g. the ratios of the flow-rates in, and the diameters of, the two daughter tubes, as well as the different angles of branching). There is, therefore, considerably more fluid mechanical information available on the subject of symmetric bifurcations, and this chapter begins with a survey of it (taken largely from the review by Pedley, 1977). It should be said at the start, however, that the problem is still very complicated, and most of the data have been obtained experimentally not theoretically, with steady rather than unsteady flow. Clearly much work remains to be done.

In all the investigations described in this section and the next, the geometry of the bifurcations is taken to be fully three-dimensional. There has been relatively extensive theoretical and experimental work on two-dimensional bifurcations, but since that geometry rules out all secondary motions it is unlikely to have much relevance to the cardiovascular system.

5.1.1 Model experiments

A full fluid dynamical description of the flow through a single junction requires the complete specification of the geometry of the junction, as well as of the flow-rate and velocity profile upstream. Thus, in addition to the diameters of the tubes, we need to know the

angles of branching, the sharpness of the flow divider, the radii of curvature of the tube walls at the junction, the way the parent tube changes shape as it approaches the bifurcation, and whether the tubes are themselves curved or straight. The experiments that have been done do not cover all possible values of the dimensionless parameters that define such a geometry. Indeed, the most detailed experiments have been done with a single geometry, chosen to be representative of bifurcations in the bronchial airways. Such a 'typical' junction is depicted in fig. 5.1, and has the following properties. (a) The diameter ratio (d_2/d_1) is 0.78, corresponding to an area ratio (both daughters to parent) of 1.2. (b) The angle of branching is 70° (qualitative experiments have been performed with different values of this and the previous parameter). (c) The flow divider is sharp. (d) The radius of curvature of the outer wall of a junction (R , fig. 5.1) lies between 1 and 30 times the radius ($\frac{1}{2}d_1$) of the parent tube. (e) As it approaches the junction, the parent tube first becomes elliptical without change of cross-sectional area, before changing both shape and area as the daughter tubes emerge. Note that the cross-sectional area at the junction is not uniquely defined, since it depends on whether the plane of measurement is perpendicular to the axis of the parent tube or that of a daughter tube. (f) Daughter tubes are initially curved and of constant area, becoming straight when the branching angle has been achieved. (The data in (c) to (f) above are all taken from Horsfield *et al.*, (1971); such detailed data are not available in arteries, even for the aortic bifurcation.) (g) Finally, we assume that the flow in the parent tube, far upstream of the bifurcation, is axisymmetric and is either Poiseuille flow or partially developed laminar entrance flow; the Reynolds number is taken to be large, of the order of 500. (Of course, the parent tube of one junction is in general the daughter of another, so the flow in it is unlikely to be symmetric.)

It is not difficult to construct a qualitative picture of the flow pattern to be expected in the daughter tube (Pedley, Schroter & Sudlow, 1971). First, the flow is split into two streams, so that a new boundary layer is formed on the inside wall, with maximum axial velocity just outside it (fig. 5.2). Secondly, the flow into each daughter tube turns a corner, so that secondary motions are set up

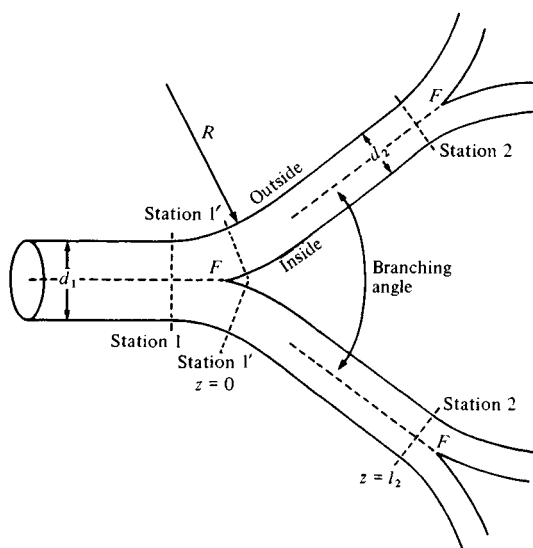


Fig. 5.1. Diagram of a 'typical' symmetric bifurcation, with a second generation downstream. F , flow dividers. Stations 1, 1' and 2 are the stations referred to in the text.

as in a uniform curved tube: the faster-moving fluid moves towards the inside wall of the junction (the outside of the bend), tending to keep the point of maximum axial velocity close to that wall, and the slower-moving fluid near the walls moves towards the outside. In addition, depending on the sharpness of the corner in the outer wall (i.e. on $2R/d_1$; see fig. 5.1), there may be a region of separated flow.

Two types of experiment have been carried out in models of single bifurcations: flow visualisation (using smoke as a tracer in air flow, or dye in water flow) and measurement of velocity profiles (using hot-wire anemometry or similar techniques). All flow-visualisation studies have confirmed the above qualitative picture, that fluid particles move downstream in the daughter tubes in two helical paths, for various branching angles, area ratios, and Reynolds numbers (in the approximate range 100–1400). Schroter & Sudlow (1969) used a 'typical' bifurcation, as described above, except that $2R/d_1$ was small ($=1$), the parent tube did not become elliptical before the junction, and the daughter tubes were not

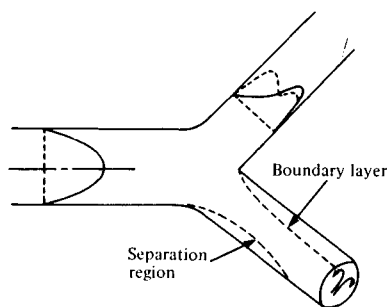


Fig. 5.2. Qualitative picture of flow downstream of a single junction with Poiseuille flow in the parent tube. Direction of secondary motions, new boundary layer and separation region are indicated in the lower branch; velocity profiles in the plane of the junction (continuous curve) and the normal plane (broken curve) are indicated in the upper branch.

initially curved (all other flow-visualisation studies have suffered from the same defects). They found that the secondary flows were strong enough to complete one cycle within three diameters of the junction. This indicates that the secondary velocities could be as high as 50% of the average axial velocities. However, the velocity measurements of Olson (1971) show that the maximum value is about 30% when $2R/d_1 = 7$, and is lower still for more gradually curved tubes (at the given branching angle of 70°). This suggests that the unnaturally sharp curvature of the outer wall is responsible for such large secondary velocities. Schroter & Sudlow also observed separation and reversed flow at the outer wall of the junction, although this does not imply a region of dead water, because the secondary motions sweep new fluid into the separation bubble from the sides (Brech & Bellhouse, 1973). Zeller, Talukder & Lorenz (1970) further confirmed that if the flow-rates in the two daughter tubes are unequal, separation readily occurs at the outer wall of the tube with the smaller flow-rate. Olson (1971) did not observe separation in his more gradually curved models, despite having the same area expansion of 1.2 as Schroter & Sudlow. Experiments on a bifurcation with a blunt flow divider suggest that even there the influence of the bifurcation on flow in the parent tube is insignificant more than one diameter upstream of the flow divider (Pacome, 1975; Pedley, Schroter & Sudlow, 1977).

The best measurements of velocity downstream of a bifurcation have been made by Olson (1971); they remain largely unpublished although a few have been reported by Pedley *et al.* (1977) and by Pedley (1977). Olson's measurements are the most reliable for the following reasons. (a) His models were more carefully made than any others, and conform closely to the 'ideal' bifurcation described above, including the gradual change in shape of the parent tube, and the initial curvature of the daughter tubes (with $2R/d_1$ equal to 7 or more). (b) He made careful measurements *both* with conventional hot-wires, which can be interpreted as measurements of axial velocity, w , as long as the component of transverse velocity normal to the wire is much less than w (in most cases this was the case), *and* with a specially designed probe consisting of two wires, one of which is given a pulse of heat and the other of which records the temperature downstream. Rotation of the probe about the pulsed wire until the response of the receiver wire is greatest gives both the magnitude and the direction of the velocity component in the plane perpendicular to the wire. Repeating the measurement at the same point in a perpendicular plane gives the complete velocity vector. Using this procedure at many points, Olson was able to map out profiles of the transverse velocity components u and v , as well as those of w . (c) Finally, Olson made measurements at more points in a given cross-section and at more cross-sections than other workers. However, because the experimental procedure was so laborious, he reported measurements of secondary velocities at only two Reynolds numbers, in one model bifurcation, and with a flat entry profile a few diameters upstream.

Typical velocities measured by Olson in the daughter tubes of the bifurcation are presented in figs. 5.3–5. Fig. 5.3 shows the development of the axial velocity profile in the plane of the bifurcation from a station 1.66 daughter-tube diameters upstream of the flow divider to many diameters downstream, at a daughter-tube Reynolds number Re_2 of 530. As expected, the maximum velocity occurs close to the inner wall of the bifurcation, although, near the flow divider, there is evidence of a slight skewing of the profile away from the inner wall, outside the boundary layer. This presumably reflects the inviscid development of the flat profile upstream as it rounds the bend (cf. § 4.4 above). Similar results were found at

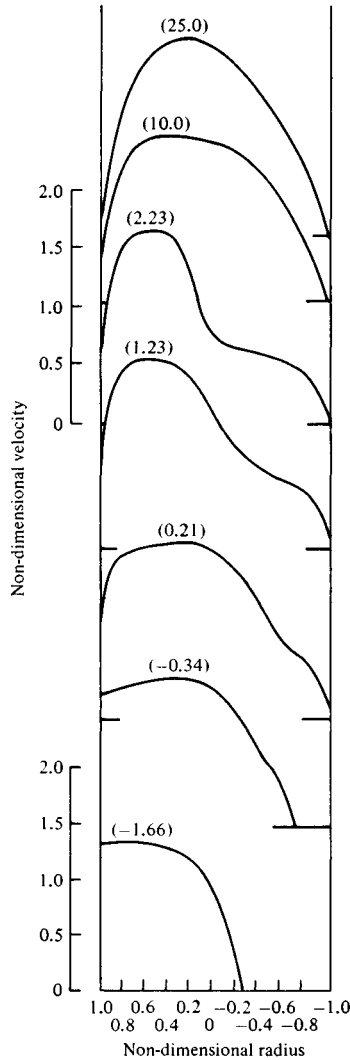


Fig. 5.3. Velocity profiles in the plane of the junction for inspiratory flow through a single bifurcation; flat entry profile, $Re = 530$. Flow divider on *left*. Figures in brackets are numbers of tube diameters from flow divider. (After Olson, 1971.)

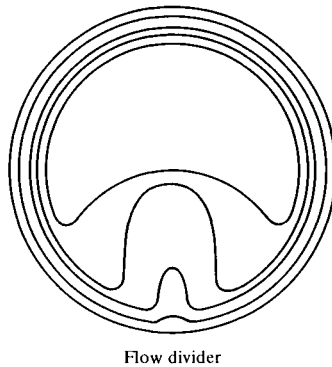


Fig. 5.4. Contour plot of axial velocity in the daughter tube at 2.2 diameters from the junction. Inspiratory flow; flat entry profile; $Re = 660$. Contours are at steps of 0.4 non-dimensional velocity (they have been slightly smoothed in reproduction). (After Olson, 1971.)

other values of Re_2 (in the range 300 to 1500). Olson found no separation from the outside wall. He also remarked that a parabolic entry profile made little difference to the results, at least after two or three diameters.

In fig. 5.4 is plotted a contour map of longitudinal velocity, measured at 2.2 diameters downstream of the flow divider and at $Re_2 = 660$. The main features are (a) that the region of high shear on the inside wall (the boundary layer) extends more than half-way round the tube, and (b) that the contours have a winged appearance, demonstrating that a velocity profile in the plane perpendicular to the bifurcation will be *M*-shaped, with a significant dip in the middle (cf. fig. 5.2).

In fig. 5.5 we reproduce Olson's measurements of the profiles of the secondary velocity components at a somewhat higher Reynolds number ($Re_2 = 935$). They are shown at four stations, three downstream and one $0.34d_2$ upstream of the flow divider. At this upstream station, the profile is plotted first in a plane perpendicular to the parent tube axis, and then in a plane perpendicular to the daughter tube axis. The difference is striking. Whereas in the first case the secondary motion is seen to be primarily towards the outside of the *junction*, in response to the change of tube shape (except on the minor axis where the effect of the imminent flow

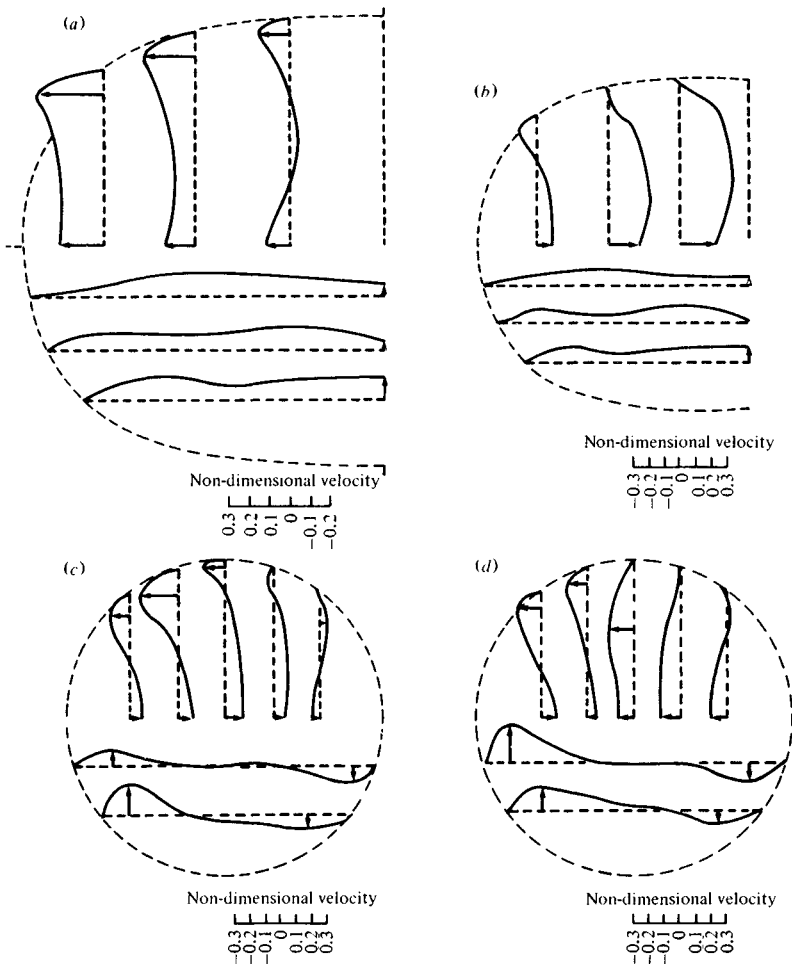


Fig. 5.5. Velocity profiles of the secondary flow at different positions upstream and downstream of the flow divider, which is on the right of the diagram; flat entry profile; $Re = 935$. (a) $0.34d$ upstream of flow divider ($d =$ diameter of daughter tube); plane of profiles is perpendicular to axis of parent tube; (b) $0.34d$ upstream; plane of profiles is perpendicular to axis of daughter tube; (c) $0.21d$ downstream; (d) $2.23d$ downstream; (e) $5.0d$ downstream. (After Olson, 1971.)

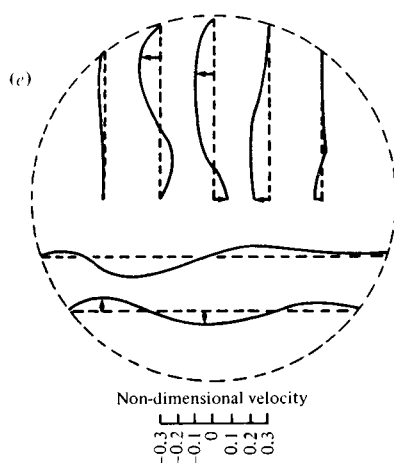


Fig. 5.5. (continued)

divider is strong), in the second case it corresponds to a strong sideways motion towards the outside of the *bend* (the flow divider). It is this aspect of the secondary flow that presents itself first to the daughter tubes, and it can be seen to persist downstream of the junction. At 0.21 diameters it is still in evidence, with a boundary layer developing at the walls in which the secondary flow back to the outside wall is to be seen, as expected from the flow-visualisation studies. Further downstream, however, at 2.23 diameters, the situation has become very confusing again; here the secondary motion is almost all directed towards the outer wall of the junction, and there is no obvious way to explain this. Further downstream still, the effect is less strong. It is as if the flow pattern varied sinusoidally with distance downstream, as has been reported for turbulent flow in pipe bends of large angle (Rowe, 1970). However, no such variation is obvious in the axial profiles.

The picture of the secondary motions in the elliptical transition region was confirmed by Olson from measurements in a tube that gradually became elliptical (with constant area), but that had no bifurcation at the other end. An example of the measurements, at a (parent tube) Reynolds number of 1620, is shown in fig. 5.6(a). The similarity between this and fig. 5.5(a) is obvious. For comparison, the corresponding plot with a parabolic entry profile is shown in fig. 5.6(b); the secondary motions are far less strong.

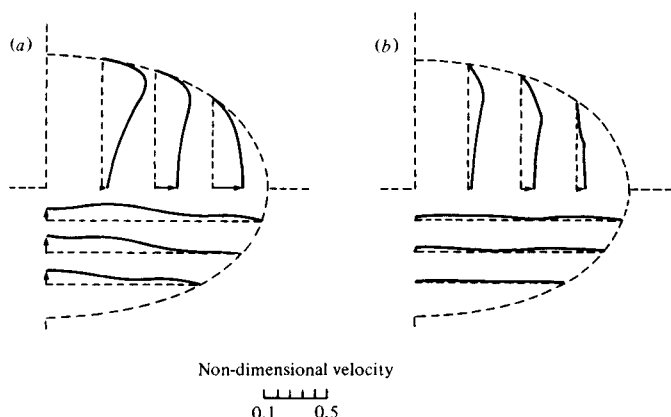


Fig. 5.6. Velocity profiles of the secondary flow in a tube that is initially circular and becomes increasingly elliptical with constant area; $Re = 1620$, (a) flat entry profile, (b) parabolic entry profile. (After Olson, 1971.)

A number of authors have made less accurate measurements in less carefully made bifurcations. Among the most important (because of the use subsequently made of them – see below) were those by Schroter & Sudlow (1969). They made hot-wire measurements of (longitudinal) velocity profiles in the plane of the junction and the plane perpendicular to it, usually with a parabolic inlet profile. They too found peak velocities near the inside wall, and an *M*-shaped profile in the plane perpendicular to the junction, and qualitatively their results differed from Olson's only in the absence of the skew outside the boundary layer on the inside wall (because the inlet profile was not flat) and in the presence of a minimum in the profile in the plane of the junction, with a second maximum near the outside wall. This they took to be associated with the separation demonstrated by their flow-visualisation experiments, since the hot-wire anemometer gives a positive signal whatever the direction of flow. Qualitatively similar results have been obtained by Schreck & Mockros (1970), Berger, Calvet & Jacquemin (1972) and Brech & Bellhouse (1973). Berger *et al.*'s measurements were made in the first generation of a branched tube network containing several generations, with the later generations still attached. It is not clear, however, what effect this might have had on the measured profiles.

A limited number of experiments have been performed in networks containing several generations of geometrically similar symmetric bifurcations, in which the length-to-diameter ratios of intermediate tubes were taken to be typical of the lung (i.e. about 3.5). Schroter & Sudlow (1969) measured profiles in a two-generation model, with one of the second-generation bifurcations being in the plane of the first and the other perpendicular to it. All the bifurcations were geometrically similar. They measured velocity profiles in the same two planes as before, at several distances from the flow divider, and at three Reynolds numbers, in each case. Berger *et al.* used a two-generation model, with all bifurcations in the same plane, and with a different area ratio at each generation, as given by the first two generations of a symmetric model of the lung proposed by Weibel (1963). Pacome extended this model to five generations, also using Weibel's data, and also keeping the first three generations coplanar, but for geometrical reasons the last two were not coplanar.

All these authors used their velocity-profile measurements in an estimate of pressure drop (see below), and the only profiles presented are in the daughters of the second bifurcation. When this is coplanar with the first, but not otherwise, the velocity fields are symmetric about the plane of the junctions, as expected. The slopes of the velocity profiles near the wall are again high at least half-way round the tube from the flow divider (note, however, that extrapolation of a measured velocity profile to zero is a notoriously inaccurate way of obtaining the shear-rate at the wall). However, the main impression is of a very complicated flow, varying significantly with distance downstream because of the redistribution of axial momentum by the secondary motions. Such disturbed (but still laminar) flow is to be anticipated almost everywhere in the lung and in much of the cardiovascular system.

Pressure drop

A quantity of fluid dynamical significance (and of great physiological importance, especially in the study of respiration) is the pressure loss associated with flow through a bifurcation. Direct measurement of the pressure in a single bifurcation does not give useful results, because the pressure differences are very small, the pressure varies

as much within the cross-section of the tube as it does across a junction (Jaffrin & Hennessey, 1972), and the contribution to the pressure drop of kinetic energy changes is large. One should therefore estimate the pressure drop by using the measured velocity profiles, and check the estimates by measuring the pressure drop across a model with several generations. Furthermore, we cannot use a momentum equation to estimate the pressure drop, because the walls of the tubes are not parallel, and so the flow divider, for example, exerts a longitudinal component of force on the flow in the parent tube (and, in any case, wall shear stress is extremely difficult to measure accurately). It is therefore necessary to use an energy equation.

We refer to a junction and its daughter tubes as a single unit (between stations 1 and 2 in fig. 5.1). The energy equation for the fluid within the unit can then be written as

$$(\hat{p}_1 + \frac{1}{2}\rho\hat{q}_1^2) - (\hat{p}_2 + \frac{1}{2}\rho\hat{q}_2^2) = D/Q, \quad (5.1)$$

where Q is the volume flow-rate through the unit, D is the total rate of viscous energy dissipation in the unit, p is pressure, q is total fluid velocity, and suffixes 1 and 2 refer to stations 1 and 2. The symbol $\hat{}$ refers to the average of a quantity, weighted by the longitudinal velocity component w , across the cross-section of the tube: thus

$$\hat{p} = \frac{1}{Q} \int p w \, dA, \quad (5.2)$$

etc. (Pedley *et al.* 1977). Note that if either p or w is uniform across the tube, then \hat{p} is equal to \bar{p} , the conventional average pressure. Also, if we write

$$\hat{q}^2 = \beta \bar{w}^2, \quad (5.3)$$

where \bar{w} is the average velocity, we note that $\beta = 1$ for parallel flow with a flat profile, and $\beta = 2$ for Poiseuille flow. For complicated three-dimensional flows such as ours, the only rational meaning that can be given to the words 'pressure drop' is that derived from (5.1) and (5.2).

In applying (5.1) to a bifurcation, two more simplifying assumptions are made. (a) We neglect the viscous dissipation at the junction itself, i.e. between stations 1 and 1', where the flow is

thought to be largely determined by non-viscous mechanisms; this is reasonable since most of the dissipation takes place in the boundary layer in the daughter tube, where the velocity gradient is high. (b) We neglect the contributions to $\widehat{q^2}$ and to D of the transverse components of velocity, u and v ; this is very crude, leading to a possible underestimate of at least 10% in D (when u and v reach 30% of \bar{w}), but no more accurate, yet still manageable, alternative has been suggested.

Pedley, Schroter & Sudlow (1970a) used rather crude interpolation procedures to estimate the dissipation per unit length (dD/dz) at each station in each daughter tube, and at each Reynolds number for which profile measurements were made. The results were expressed as the ratio, Y , of the actual dissipation-rate to that for Poiseuille flow at the same Reynolds number in the same tube. D was calculated from dD/dz , and its ratio, Z , to the corresponding Poiseuille-flow value was reported. The results showed considerable scatter, but two general conclusions could be drawn: Y (i.e. dD/dz) decreased on average with increased distance, z , from the flow divider; both Y and Z decreased (on average) as Re decreased. Because most of the energy dissipation is expected to take place in the boundary layer growing on the flow divider, these authors proposed a model in which Y and Z would depend on Re , z , and the tube length, l , and diameter, d , in the same way as for entry flow in a straight tube. According to this model, Y and Z in any tube would be given by

$$Y = \frac{1}{2}\gamma(Re\,d/z)^{1/2}, \quad Z = \gamma(Re\,d/l)^{1/2}, \quad (5.4)$$

where the dimensionless constant γ is independent of Re , z , l , and d . These equations can be used to deduce values of γ from the values of Y and Z derived from the measured velocity profiles. Pedley *et al.* (1970a) found no systematic dependence of the values of γ obtained in this way on either Re or z/d (l/d was constant in the experiments), and therefore regarded the entry flow model as confirmed. The only systematic variation was that the values of γ obtained from second-generation tubes were uniformly smaller than those obtained from the first, by 25% on average. This indicates that greater complexity in the flow modifies the boundary layer on the flow divider. Nevertheless, this error was within two

standard deviations, and the authors chose to use their overall mean value of $\gamma = 0.33$ for predictions of energy dissipation in the lung. Those predictions were in good qualitative agreement with physiological experiment (Pedley, Schroter & Sudlow, 1970*b*).

The values of β (see (5.3)) obtained from the measured profiles at a distance of 6 cm from the flow divider (close to station 2, fig. 5.1) showed *no* systematic variation with Re or with generation number, and the average value of 1.7 was used in all predictions.

The above results concerning dissipation suggest that in any system of symmetric branched tubes, with the same branching angle and area ratio, and with Reynolds numbers in the same range, D will be proportional to $Q^{5/2}$, and the loss of total head, averaged as in (5.1) and (5.2), will be proportional to $Q^{3/2}$. Berger *et al.* (1972) obtained conflicting results by a similar method. They found that a good fit to their data is given by $D \propto Q^2$, so that the loss of total head is directly proportional to Q . Such a linear relation is inherently very unlikely, although the constant of proportionality is much greater than in Poiseuille flow, and as yet it has not proved possible to explain the discrepancy (Pedley, 1977). However, it is interesting to note that a student of Calvet's, Pacome (1975), has extended the measurements of Berger *et al.* to five generations, but he measured pressure drops as well as velocity profiles (the lateral variations in pressure are small compared with the overall pressure drop in a network of this size). His most important result was that, when the kinetic energy terms ($\frac{1}{2}\beta\rho\bar{w}^2$) in (5.1) are correctly accounted for, the total head loss (D/Q) is accurately proportional to $Q^{3/2}$. This vindicates the model of Pedley *et al.* (1970*a*), even if doubts remain about the estimation of dissipation.

Berger *et al.* also disagreed with Pedley *et al.* in the value to be taken for the kinetic energy factor β . They found a value lying between 1.44 and 1.55 in generation 1, and between 1.09 and 1.29 in generation 2, and being in general lowest for the highest Reynolds numbers: the parent-tube Reynolds number took several values between 420 and 2800, at the highest of which the flow was turbulent. Douglass (1973) on the other hand found values of β around 2.0 in generation 1, and around 1.5 in generation 2, for turbulent flow at $Re > 10^4$, with no systematic dependence on Re .

All these discrepancies suggest that further experiments are still required.

Finally we may note that a few measurements have been made on unsteady laminar flow in model branched tubes. Jaffrin & Hennessey (1972) measured the variation of static pressure at several sites in a two-generation model when the flow-rate was varied sinusoidally. The peak values of Re and the Womersley parameter in the parent tube were taken to be 1560 and 2.7 respectively in one case, and 1230 and 1.9 in another. There was a small phase shift between pressure drop and flow-rate at the higher frequency, but no amplitude response. The measurements confirmed that transverse pressure variations in a daughter tube are as great as the longitudinal variations in two generations. The pressure drop for expiratory flow was greater than that for inspiration. Brech & Bellhouse (1973) measured velocity profiles and shear stresses in pulsatile flow (with non-zero mean) through a single bifurcation, with parent-tube Re equal to 750 and 1500, and α equal to 22. However, they reported that the flow was quasi-steady, which at such a large value of α is extremely difficult to believe and casts some doubt on the accuracy of their measurements.

5.1.2 *Theory*

Attention is still restricted to steady laminar flow at high Reynolds number. The geometrical configuration of even a single bifurcation is so complicated that a complete analytical theory is out of the question, and we must await the development of suitable numerical methods before we can investigate all the details of the flow. (The flow in two-dimensional bifurcations has been analysed numerically, but since that inevitably excludes all the interesting phenomena, and gives no clue to the structure of the three-dimensional flow even in an idealised example (Smith, 1977*a*), it is not worth describing the results. One hopes that the methods can soon be extended to three-dimensional bifurcations.) Theoretical insight into the development of the secondary motions and the distortion of the axial velocity profile will be possible only with the help of crude simplifying assumptions, which must always be assessed critically. One such is to neglect the effect of viscosity on the gross changes in the core flow that take place in the region of the

junction itself, on the grounds that viscosity has no time to influence the flow pattern except in the boundary layers. This is likely to be reasonable for a short distance beyond the junction, as long as separation does not occur, and will break down where secondary motions cause fluid from near the wall to penetrate into the core from the outside of the bend. The development of the boundary layers, both on the flow divider in the daughter tubes, and upstream of the junction in the parent, may be analysed separately.

Olson's observations on the flow in the elliptic transition region suggest that the non-viscous core problem can also be divided into two stages. First, one should compute the secondary motions (and the distortion of the axial velocity profile) caused by streamline curvature in the increasingly elliptic parent tube upstream of the flow divider. This neglects any blocking effect that the presence of the flow divider may have on the core flow just upstream, in the hope (based on the flow-visualisation studies reviewed above), that this is confined to a small region, especially when the flow divider is sharp. Secondly, one should calculate the effect that the initial curvature of the daughter tube will have on the already distorted flow entering it.

A tentative start has been made to the first stage by Sobey (1976*a*), who has calculated the distortion of a weakly sheared axisymmetric flow in a tube that is circular (radius a_0) for $z < 0$, and that has slowly varying (but not necessarily small) ellipticity downstream ($z > 0$). He solved the problem using classical secondary flow methods (reviewed by Horlock & Lakshminarayana, 1973), which involve the following stages:

(i) Calculate the potential flow in the slowly varying tube as a power series in ε (equal to a_0/l , where l is the length-scale for longitudinal variations). The leading term is a uniform stream with velocity equal to \hat{W}_0/ab , where \hat{W}_0 is the average velocity in $z < 0$, and $a_0a(z)$, $a_0b(z)$ are the major and minor axes of the elliptical cross-section. The next term in the velocity potential, of order ε , can easily be calculated, and is determined uniquely by the condition that volume flux is uniform along the tube. The error term is $O(\varepsilon^3)$.

(ii) Let the transverse vorticity in the upstream flow be $O(\delta\hat{W}_0/a_0)$, where $\delta = o(\varepsilon)$; then the streamlines of the $O(\varepsilon)$ potential flow will be a first approximation to the actual streamlines.

Assuming that vortex lines are carried along the potential flow streamlines one can compute a first approximation to the disturbance vorticity field. This includes longitudinal components, which are associated with secondary velocity components, of $O(\hat{W}_0 \varepsilon \delta)$, as well as an $O(\hat{W}_0 \delta)$ perturbation to the axial velocity.

(iii) These result in further distortions to the axial velocity profile, of $O(\hat{W}_0 \delta^2)$, which can also be computed without too much difficulty.

This approximation procedure is self-consistent for values of z less than $O(a_0/\varepsilon \delta)$. Its greatest weakness is that it cannot treat large, $O(\hat{W}_0/a_0)$, upstream vorticity, and therefore any results can have at most qualitative relevance to real pipe flows, except perhaps those (as in some of Olson's experiments) with almost flat velocity profiles and thin boundary layers at the inlet.

Sobey's results can be summarised quite simply. When the entry profile is perfectly flat, the secondary velocity profiles are also flat, and these motions are stronger further away from the centre of the tube. The contours of constant axial velocity are ellipses that remain similar to the tube itself. When there is a slight shear, the secondary velocities are greater near the wall of the tube, and the contours of constant axial velocity are distorted so that the axial velocity is increased near the ends of the major axis, and decreased near the ends of the minor axis. The predicted secondary profiles agree qualitatively with those of fig. 5.6(a), except, of course, in the boundary layers on the walls.

An extremely crude estimate of the flow in the (straight) daughter tubes of a symmetrical bifurcation has been made by Scherer (1972), who ignored any perturbation to the flow in the parent tube upstream of the flow divider. He also assumed that the flow in the daughter tubes did not change with distance along them, and then calculated the simplest possible flow pattern consistent (i) with this assumption, (ii) with the non-viscous equations of motion, and (iii) with the fact that the flow must be symmetric about the plane containing the axes of all tubes in the bifurcation. The flow entering from the parent tube was taken into account by arranging that the axial and transverse velocity components on the axis of the daughter tube at its entrance were the same as would occur at that point if the parent tube continued uninterrupted. He worked out the details

for a flat entry profile, of velocity \hat{W}_0 , and his results are in rough qualitative agreement with Schroter & Sudlow's profiles, including the *M*-shaped profile in the plane normal to that of the junction.

Before further progress can be made on the core flow problem a theory will have to be developed to analyse the rapid inviscid distortion, over a short length of tube, of a flow with large transverse vorticity. It is difficult to see how any perturbation theory (such as Sobey's) can suffice.

Progress has also been made with the boundary layer analysis, though this is necessarily restricted to an idealised situation in which the core flow is not grossly distorted by secondary vorticity. Smith (1977*a*) examined the effect of dividing the flow into two without making it simultaneously turn a corner, by considering steady flow in an infinitely long, straight pipe of circular cross-section with radius a_0 (whose axis is the line $x = y = 0$) which is split by a semi-infinite plane $x = 0$ in $z > 0$. Poiseuille flow

$$w = W_0(x, y) \equiv \frac{1}{4}(1 - x^2 - y^2), \quad p = p_0 - z, \quad (5.5)$$

is present as $z \rightarrow -\infty$; here x, y, z are made dimensionless with respect to the tube radius a_0 , and the velocity and pressure are non-dimensionalised with respect to \hat{W}_0 (equal to 4 times the centre-line velocity) and to $\hat{W}_0\mu/a_0$ (equal to a_0 times the upstream pressure gradient) respectively. Smith analyses the flow on a long, boundary layer length-scale, $z = O(Re)$, where $Re = \hat{W}_0a_0/\nu$, but focusses attention on small values of $Z = z/Re$; at large values of Z the flow will tend towards the form of Poiseuille flow appropriate to tubes of semi-circular cross-section. A Blasius-type boundary layer is set up on the splitter plate, corresponding to the y -dependent outer velocity $w = \frac{1}{4}(1 - y^2)$. This generates a y -dependent normal velocity u which causes both a displacement of the inviscid core flow and a transverse velocity v inside the boundary layer and in the core. The net effect of these secondary motions is to transport fluid from the outer corner of the tube ($x = 0, y = 1$; see fig. 5.7) to the point of symmetry on the wall ($x = 1, y = 0$). Such a flow, however, cannot satisfy the equation of continuity unless there is an acceleration of the axial flow in the core near the point of symmetry, and this requires the presence of an additional axial pressure gradient of $O(Z^{-1/2})$. The associated pressure is itself responsible for a

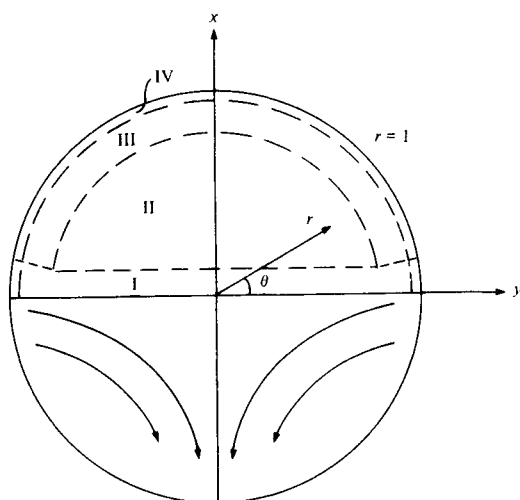


Fig. 5.7. Diagram of the four principal regions of the flow, with coordinate system and sketch of secondary flow direction in the inviscid core (region II). The flow divider occupies the plane $x = 0$ ($\theta = 0, \pi$).

vigorous secondary motion in a boundary layer near the outer wall ($r = (x^2 + y^2)^{1/2} = 1$), which turns out to have a double structure, with an outer, inviscid region of thickness proportional to $Z^{1/4}$, and an inner viscous region of thickness proportional to $Z^{3/8}$ to reduce the tangential velocity to zero. We outline Smith's solution in the four principal regions of the flow, shown schematically in fig. 5.7.

The expectation of a Blasius-type boundary layer indicates that the variables should be rescaled according to

$$(u, v) = Re^{-1}(U, V), \quad w = w, \quad p = ReP$$

for $Z = O(1)$. The governing equations then are

$$\left. \begin{aligned} U_x + V_y + w_Z &= 0, \\ U w_x + V w_y + w w_Z &= -P_Z + \nabla^2 w, \\ U \Omega_x + V \Omega_y + w \Omega_Z - \Omega w_Z - w_x U_Z + w_y V_Z &= \nabla^2 \Omega, \end{aligned} \right\} \quad (5.6)$$

where $\nabla^2 = \partial^2/\partial x^2 + \partial^2/\partial y^2$, Ω is the axial component of vorticity,

$$\Omega = -U_y + V_x,$$

and the pressure $P(Z)$ is independent of x and y .

The Blasius boundary layer, region I

Here the z - and x -components of velocity are given by the standard Blasius theory, and are

$$\left. \begin{aligned} w &= \frac{1}{4}(1-y^2)f'_0(\tilde{\eta}) + O(Z^{1/2}), \\ U &= Z^{-1/2}[\frac{1}{8}(1-y^2)]^{1/2}(\tilde{\eta}f'_0 - f_0) + O(1), \end{aligned} \right\} \quad (5.7)$$

where

$$\tilde{\eta} = xZ^{-1/2}[\frac{1}{8}(1-y^2)]^{1/2}$$

and $f_0(\tilde{\eta})$ is the Blasius function. Associated with this flow is a transverse component of velocity,

$$V = v_0(\tilde{\eta}, x) + O(Z^{1/2}),$$

which can readily be calculated. This does not tend to zero as $\tilde{\eta} \rightarrow \infty$, but is given instead by

$$v_0 \sim -3\beta_0 y \tilde{\eta} / (1-y^2) + O(1), \quad (5.8)$$

where

$$\beta_0 = \lim_{\tilde{\eta} \rightarrow \infty} (f_0 - \tilde{\eta}) > 0.$$

Thus there must also be a secondary core flow which is directed in towards the centre of the plate. The pressure perturbation mentioned above does not affect the flow region I to this order; it turns out that a self-consistent structure to the flow elsewhere can be formulated only if

$$dP/dZ = P_1 Z^{-1/2} + O(Z^{-1/4}), \quad (5.9)$$

where P_1 is a constant.

The core, region II

The Z -dependence of the above solutions as $Z \rightarrow 0+$ suggests that the perturbation to the oncoming flow in the core takes the form

$$w = W_0(x, y) + Z^{1/2}W_1, \quad U = Z^{-1/2}U_1, \quad V = Z^{-1/2}V_1.$$

Substitution into the governing equations (5.6) shows that U_1 , V_1 and W_1 satisfy linearised inviscid disturbance equations that have a solution of the form

$$(U_1, V_1) = \frac{1}{W_0} \left(\frac{\partial \phi}{\partial x}, \frac{\partial \phi}{\partial y} \right), \quad W_1 = -\frac{8}{1-r^2} \left(\nabla^2 \phi + \frac{2r}{1-r^2} \frac{\partial \phi}{\partial r} \right), \quad (5.10)$$

where

$$(1-r^2)\nabla^2\phi + 4r\partial\phi/\partial r = P_1(1-r^2) \quad (5.11)$$

and

$$\phi \sim \gamma x(1-y^2)^{3/2} \quad \text{as } x \rightarrow 0. \quad (5.12)$$

Here $\gamma = \beta_0/8\sqrt{2}$ and (r, θ) are polar coordinates in the transverse plane (fig. 5.7). The condition (5.12) determines ϕ uniquely; the only boundary condition that is satisfied on $r = 1$ is $\partial\phi/\partial r = 0$, which follows from (5.11).

For a given value of P_1 , the problem for ϕ can, in principle, be solved; a method for doing so is given by Smith. This inviscid solution, of course, does not satisfy the no-slip condition on $r = 1$: if $A_0(\theta)$ stands for the unknown value of ϕ at $r = 1$, then (5.11) shows that

$$\phi = A_0(\theta) + \frac{1}{2}(1-r^2)[A_0''(\theta) - P_1] + O[(1-r)^3]$$

as $r \rightarrow 1$. The corresponding velocity components are

$$\begin{aligned} w &\sim \frac{1}{2}(1-r) - 4Z^{1/2}A_0''(\theta)/(1-r) + \dots \\ U^* &\sim -2Z^{-1/2}(A_0'' - P_1) + \dots, \quad V^* \sim [2Z^{-1/2}/(1-r)]A_0'(\theta), \end{aligned} \quad (5.13)$$

where we have introduced velocity components in the r - and θ -direction such that

$$U^* = (Z^{-1/2}/W_0)\partial\phi/\partial r, \quad V^* = (Z^{-1/2}/W_0)(1/r)\partial\phi/\partial\theta.$$

We note that this solution breaks down when the second term in w becomes comparable with the first, which occurs when $1-r = O(Z^{1/4})$. A boundary layer must therefore be interposed at this distance from the wall.

For future reference it is useful to write down the forms taken by the function $A_0(\theta)$ at small values of θ and of $\alpha = \frac{1}{2}\pi - \theta$. Series solutions of the problem for ϕ lead to

$$A_0(\theta) \sim \frac{1}{2}P_1\theta^2 + \frac{8}{5}\gamma\theta^{5/2} - \frac{1}{6}P_1\pi\theta^3 + O(\theta^{7/2}) \quad (5.14)$$

and

$$A_0(\theta) \sim A_0(\frac{1}{2}\pi) - \kappa\alpha^2 + O(\alpha^4), \quad (5.15)$$

where κ is a constant depending on γ and P_1 , and

$$A_0(\frac{1}{2}\pi) = 0.241 P_1 + 0.721 \gamma.$$

The inertial and viscous side-wall layers, regions III and IV

Here the appropriate normal coordinate is $\zeta = (1-r)Z^{-1/4}$, and (5.13) shows that the corresponding scaling for the velocity components is

$$w = Z^{1/4}w_1(\zeta, \theta), \quad U^* = Z^{-1/2}u_1(\zeta, \theta), \quad V^* = Z^{-3/4}v_1(\zeta, \theta).$$

Symmetry considerations mean that only the range $0 < \theta < \frac{1}{2}\pi$ need be considered. Substituting into (5.6) and retaining only the leading term as $Z \rightarrow 0+$, we find that the governing equations in region III are inviscid, and represent a non-linear interaction between fluid inertia and the pressure gradients in the axial and azimuthal directions (represented by P_1 and $\frac{1}{2}A'_0(\theta)$). The no-slip condition cannot be satisfied at $\zeta = 0$, the only condition that can be imposed there being that of zero normal velocity u_1 . Thus as $\zeta \rightarrow 0$ the following representation of the flow is anticipated:

$$w_1 \sim C(\theta), \quad u_1 \sim \zeta D(\theta), \quad v_1 \sim E(\theta),$$

where C, D, E are functions of θ to be found. Putting $\zeta = 0$ in the governing equations shows that they satisfy

$$\left. \begin{aligned} \frac{1}{4}C &= D - E', \\ \frac{1}{4}C^2 + EC' &= -P_1, \\ \frac{3}{4}CE - EE' &= \frac{1}{2}A'_0. \end{aligned} \right\} \quad (5.16)$$

The viscous terms in the equations of motion become as large as the inertia terms when $(1-r) = O(Z^{3/8})$; a viscous sublayer on this scale will enable the no-slip condition to be satisfied. The appropriate equations in this sublayer (region IV) are obtained by setting

$$w = Z^{1/4}\tilde{w}(\eta, \theta), \quad U^* = Z^{-3/8}\tilde{u}(\eta, \theta), \quad V^* = Z^{-3/4}\tilde{v}(\eta, \theta),$$

where $\eta = (1-r)Z^{-3/8}$; the outer boundary conditions are

$$\tilde{w} \rightarrow C(\theta), \quad \tilde{u} \sim \eta D(\theta), \quad \tilde{v} \sim E(\theta) \quad \text{as } \eta \rightarrow \infty.$$

Note that the above scaling predicts values of the wall shear that are much greater than those in the oncoming Poiseuille flow, being $O(Z^{-1/8})$ as $Z \rightarrow 0+$.

Smith (1977a) has not obtained a full numerical solution to the non-linear partial differential equations governing the flow in regions III and IV. However, he has answered the most important

questions, which are whether there can be a solution of the proposed form, and if so how the unknown induced pressure gradient term can be determined. He makes it very plausible that a solution for the viscous layer (region IV) can be found for any negative value of P_1 . What determines P_1 is the condition that the swirl velocity component V^* should be zero at each end of the boundary layers in regions III and IV (i.e. at $\theta = 0$ and $\theta = \frac{1}{2}\pi$). He does not *prove* that there cannot be a very rapid change of secondary flow direction in a small region near the corner $\theta = 0$, $r = 1$, but if a solution can be found for which this is merely a region of passive adjustment, then it is reasonable to expect it to be correct. Thus the function $E(\theta)$ derived from (5.16) is taken to vanish at both $\theta = 0$ and $\theta = \frac{1}{2}\pi$.

The nature of the solutions of (5.16) near $\theta = 0$ can be obtained with the help of (5.14). It is necessary that P_1 be negative (i.e. the induced pressure gradient is favourable, leading to the expected increase in pressure drop over that in undisturbed Poiseuille flow), and the following relations emerge:

$$C(\theta) \rightarrow C_0, \quad D(\theta) \rightarrow D_0, \quad E(\theta) \sim E_1(\theta) \quad \text{as } \theta \rightarrow 0+,$$

where

$$C_0 = 2|P_1|^{1/2}, \quad D_0 = \frac{1}{4}(5 - \sqrt{17})|P_1|^{1/2}, \quad E_1 = \frac{1}{4}(3 - \sqrt{17})|P_1|^{1/2}. \quad (5.17)$$

The choice of sign of the square root is discussed below. An expansion in integer powers of $\theta^{1/2}$, which is valid as long as there is no singular behaviour in the corner, shows that $C \equiv C_0$. This is confirmed by an expansion in powers of $\alpha = \frac{1}{2}\pi - \theta$, which with the help of (5.15), gives

$$C \equiv \bar{C}_0, \quad D \rightarrow \bar{D}_0, \quad E \sim \alpha \bar{E}_1 \quad \text{as } \alpha \rightarrow 0+,$$

where

$$\bar{C}_0 = 2|P_1|^{1/2}, \quad \bar{D}_0 = \frac{1}{4}|P_1|^{1/2}[5 - (9 - 16\kappa/P_1)^{1/2}], \\ \bar{E}_1 = \frac{1}{4}|P_1|^{1/2}[-3 + (9 - 16\kappa/P_1)^{1/2}].$$

The last of equations (5.15), with $C \equiv 2|P_1|^{1/2}$, leads to the following non-linear ordinary differential equation for $E(\theta)$:

$$(\frac{3}{2}|P_1|^{1/2} - E')E = \frac{1}{2}A_0'.$$

This can be solved in $\theta > 0$, subject to the condition that $E \sim E_1\theta$ as $\theta \rightarrow 0+$, for all values of P_1 , since when P_1 is fixed, $A_0(\theta)$ is

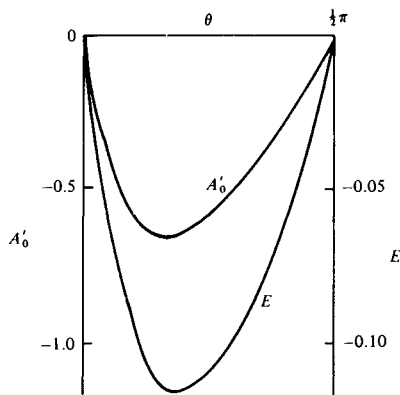


Fig. 5.8. Solution curves for the swirling velocities $A'_0(\theta)$, $E(\theta)$ at the outer edges of layers III and IV respectively ($P_1 = -3.35$). (After Smith, 1977*a*.)

determined from the solution of (5.11) and (5.12). The condition $E(\frac{1}{2}\pi) = 0$ then serves to determine P_1 ; Smith's numerical solution eventually yields the unique value $P_1 = -3.35$. The corresponding solutions for $E(\theta)$ and $A'_0(\theta)$, representing the swirl velocity at the inner and the outer edges of region III respectively, are shown in fig. 5.8.

These curves suggest that the swirl velocity is always in the same sense in region III, and this is confirmed by detailed solutions for small θ and for small α . However, solution of the equations for the viscous layer IV at both small θ and small α shows that the swirl velocity very near the wall is in the opposite sense to that in region III and the core. This indicates that there is a region of closed secondary streamlines near the wall, represented schematically in fig. 5.9; it should also be remembered that the magnitude of the swirl velocity in regions III and IV is very large compared with that in the core, being $O(Z^{-3/4})$. The region III and IV solutions also give the clue as to why the negative root $-\sqrt{17}$ was chosen in (5.17). Choice of the positive root would have implied an extra change of sign of swirl velocity in region III, in addition to the change of sign in region IV, and there seems to be no physical reason for this. However, there is not yet a mathematical or numerical demonstration that the positive root does not correspond to a self-consistent solution, and the possibility of non-uniqueness cannot be ruled out.

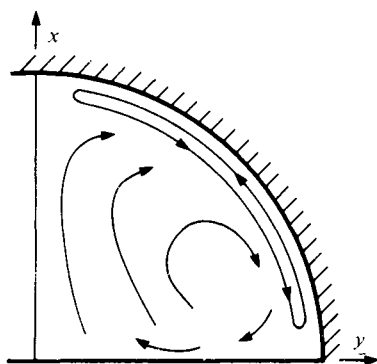


Fig. 5.9. Representative diagram of the induced secondary motion in one-half of a daughter tube. The flow velocities within the vortices adjoining the curved wall are much greater than within the core. (After Smith, 1977a.)

Another feature of the present solution worth noting is that the predicted secondary motion in the core is in the opposite sense to that which would be generated by curvature of the daughter tubes away from the junction. The experimental observations described in § 5.1.1 therefore demonstrate that the curvature present in the model bifurcations is a much more potent source of secondary motion than the branching *per se*, as analysed here.

Final validation of the flow structure outlined above will depend on a solution being obtained for the transition region, corresponding to the scale $z = O(1)$, between the upstream Poiseuille flow and the downstream boundary layer flow investigated here. Smith (1977a) has not attempted such a solution, but the flow 'far' upstream ($z \rightarrow -\infty$) will presumably be a small perturbation to Poiseuille flow, and can therefore be described by an analysis such as that used both in § 4.5 for flow entering a bend (Smith, 1976b) and in § 5.2.2 below for flow upstream of a weak side-branch, as represented by (5.21) (Smith, 1976c). Although such an analysis is linearised, it does indicate a tendency towards three-dimensional flow separation at a distance $O(a_0 \log Re)$ upstream of a non-axisymmetric deformation (such as branching) in a straight tube. Smith (1977b) has analysed upstream separation in two-dimensional channels and in axisymmetrically distorted tubes, but not yet in the non-axisymmetric conditions of interest here. His

axisymmetric results, however, are likely to be relevant to the flow upstream of a symmetric arterial stenosis, of either natural or artificial origin. An important conclusion is that the core flow at $O(a_0)$ upstream of a severe obstruction will be quite different from the Poiseuille flow assumed to be present far upstream.

5.2 Flow in asymmetric bifurcations

5.2.1 Model experiments

Flow visualisations and velocity profile measurements downstream of various asymmetric bifurcations have been made by Talukder (1975) and by Talukder & Nerem (1978) who have considerably extended the earlier results of Zeller *et al.* (1970). There are three possible causes of asymmetry in the flow through a single bifurcation (fig. 5.10), even if the velocity profile far upstream in the parent tube is axisymmetric. These are: different areas of the daughter tubes ($A_1 \neq A_2$), different angles of branching ($\theta_1 \neq \theta_2$), and different flow-rates ($Q_1 \neq Q_2$). Talukder's (1975) experiments compared an asymmetric model ($\theta_1 = 15^\circ$, $\theta_2 = 30^\circ$, $A_1/A_2 = 2.12$, $A_1 + A_2 = 1.2 A_0$) with two symmetric models ($\theta_1 = \theta_2 = 15^\circ$ and 30° respectively; $A_1 + A_2 = 1.2 A_0$), while his more recent work has examined right-angle branches off a straight tube ($\theta_1 = 0^\circ$, $\theta_2 = 90^\circ$, $A_1 = A_2 = A_0$). In each case he has considered steady flow with various flow-rate ratios (Q_1/Q_2) and parent-tube Reynolds numbers, and has also made limited observations on unsteady flow. Talukder's work is intended to be applied to predicting the flow patterns and wall shear stress in large arteries, in particular to the junctions between the aorta and vein grafts which are used surgically to by-pass diseased coronary arteries. Some flow visualisations have also been made on flow in right-angle junctions by Dr Elspeth Brighton and Dr C. D. Bertram, with intended application to the avian respiratory system. In all cases the flow far upstream of the branch was fully developed, i.e. was Poiseuille flow when steady.

The main features of steady flow, as observed by flow visualisation, can be described qualitatively as follows. Except when one of the branching angles is zero, the streams of fluid into each branch have to change their direction, as in a symmetric bifurcation. Thus

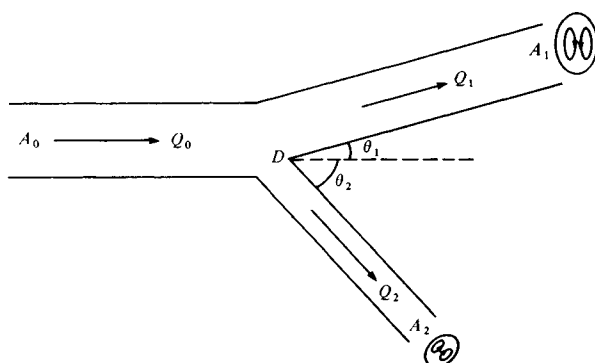


Fig. 5.10. Sketch of an asymmetric bifurcation, showing some of the parameters that must be specified.

secondary motions are generated in each stream by the same mechanism as in a curved tube, and the peak velocity is maintained near the outside bend of each stream. Even when one of the branching angles is zero, as in the case of a right-angled branch off an otherwise undisturbed parent tube, the motion near the walls of the parent tube has a complicated three-dimensional structure, and secondary motions are observed. For example, if the flow-rate down the side-branch in a right-angle junction is comparable with that in the straight branch, fluid particles that are initially near the far wall of the parent tube are carried transversely, in the boundary layer still, towards the side-branch. However, they may travel some way down the straight branch before turning back, eventually to enter the side-branch (fig. 5.11). Thus it is clear that the dividing stream surface can intersect the tube walls in a very complicated curve, which would defy detailed quantitative description. Only in the plane of symmetry is it possible to say that the dividing stream surface intersects the walls somewhere near the 'flow divider' (D in fig. 5.10), the exact position depending on the flow-rate ratio.

Another almost universal feature of the flow, absent in many symmetric bifurcations, is flow separation. This occurs *either* because a fluid stream has to negotiate a sharp corner, as at S_1 in fig. 5.12(a), *or* because there is sideways flow requiring a relatively strong transverse pressure gradient away from a boundary, which causes a pressure rise on the boundary and hence an adverse

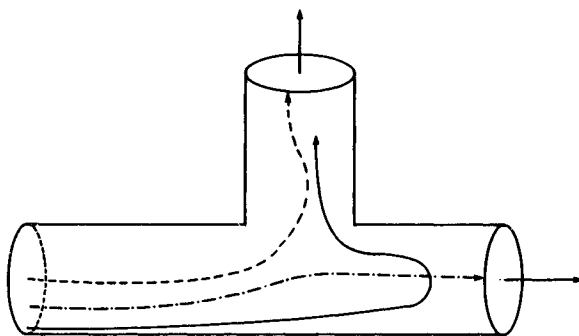


Fig. 5.11. Sketch of streamlines in steady flow in a T-junction, when the flow-rates in the two daughter tubes are comparable. Continuous curve, streamline near wall, remaining close to it; broken curve, streamline near centre line of parent tube; dot-dash curve, streamline between the two.

pressure gradient for flow along the boundary (S_2 in fig. 5.12(a), S_3 in fig. 5.12(b)). In all cases studied, the separation bubbles are bounded downstream, where the flow re-attaches, and away from the plane of symmetry, where the top and bottom boundary layers are continuous from parent tube to daughters. If regions of low wall shear are predisposed to the development of atherosclerosis (§ 1.2), then such flow-separation zones are likely to be dangerous, and it is important to have some idea of where they might occur in the circulation. In particular, surgical techniques such as vein grafting should be designed to avoid post-operative flow separation, especially when it is associated with dead-water regions, as in these steady flows. Observation of pulsatile flow in such models showed vigorous oscillatory movements in the dead-water regions, resulting in a more rapid turnover of fluid there; this would presumably be beneficial *in vivo*.

Talukder & Nerem (1978) have made velocity-profile measurements only in steady flow and only in the plane of the bifurcations. The best measurements were those made with a hot-film anemometer in the right-angled model, and are reproduced in figs. 5.13 to 5.15. The measurements are made in the side-tube at various parent and daughter-tube flow-rates, and all show a consistent pattern. A separated region is clearly present at one diameter from the junction, but by 2.5 diameters re-attachment has occurred, and,

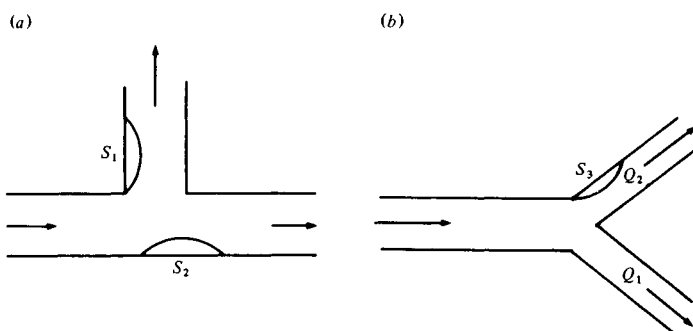


Fig. 5.12. Regions where separation is observed (a) in a T-junction, (b) in a symmetric junction with unequal flow rates ($Q_1 > Q_2$).

at least at the lower side-tube Reynolds number of 100, the velocity profile is remarkably close to its ultimate parabolic form. Very similar mean velocity profiles have been measured in vein grafts interposed (at 90°) between the iliac arteries of experimental dogs, indicating the practical relevance of these experiments (Rittgers *et al.*, 1976). It is interesting to note that the dead-water region appears to persist much further downstream in vein grafts that have been implanted for four months than in those implanted just before the measurements were made. This appeared to be associated with a chronic increase in internal diameter of about 50%, rather than with distortion of the junction wall by atheroma or other abnormalities.

Talukder (1975) also used a hot-film probe to measure wall shear stress at three sites in the daughter tube of a bifurcation with symmetric geometry and with symmetric or asymmetric flow-rates. In addition, he measured wall shear in the parent tube at a site about seven diameters upstream from the bifurcation, confirming in steady flow that the ratio between the actual wall shear and that predicted for Poiseuille flow at the same Reynolds number is very close to 1, but increases very gradually with Reynolds number. His measurements downstream of the bifurcation in steady flow, when the flow-rate through the branch where measurements were being made was only 30% of the total, showed a marked reduction below the Poiseuille value, especially at higher Reynolds numbers (500–1000 rather than 100–200). This is interpreted as evidence of a

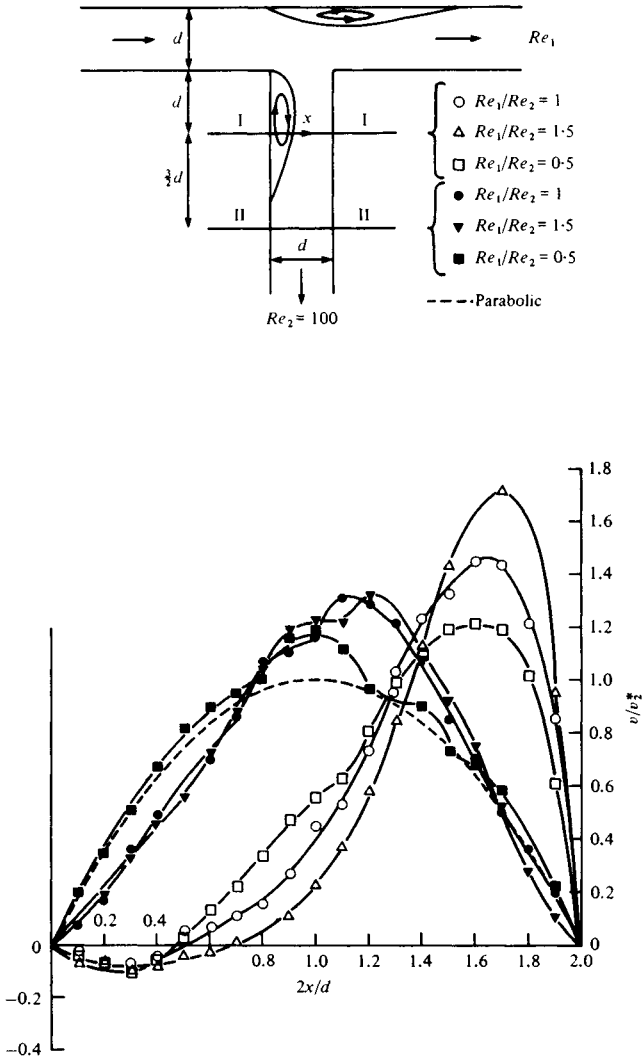


Fig. 5.13. Axial velocity profiles measured in the side-branch of a T-junction by Talukder & Nerem (1978). Re_1 , Re_2 are the Reynolds numbers in the daughter tubes; v_2^* is the average velocity in the branch. Details given in diagram.

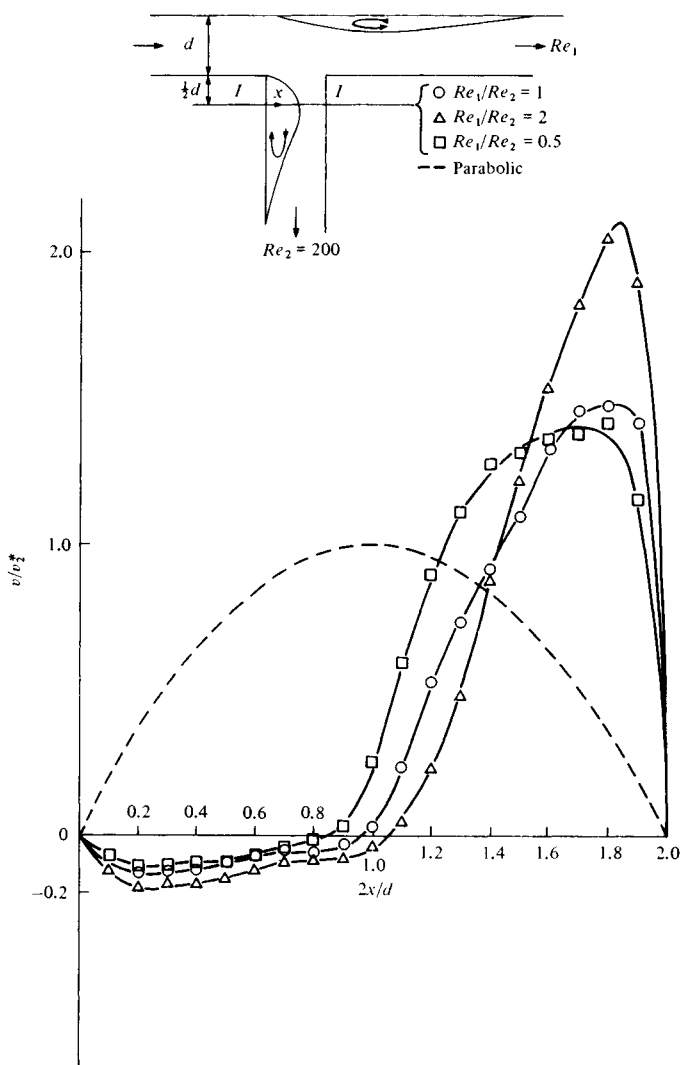


Fig. 5.14. Axial velocity profiles measured in the side-branch of a T-junction by Talukder & Nerem (1978). Re_1 , Re_2 are the Reynolds numbers in the daughter tubes; v_2^* is the average velocity in the branch. Details given in diagram.

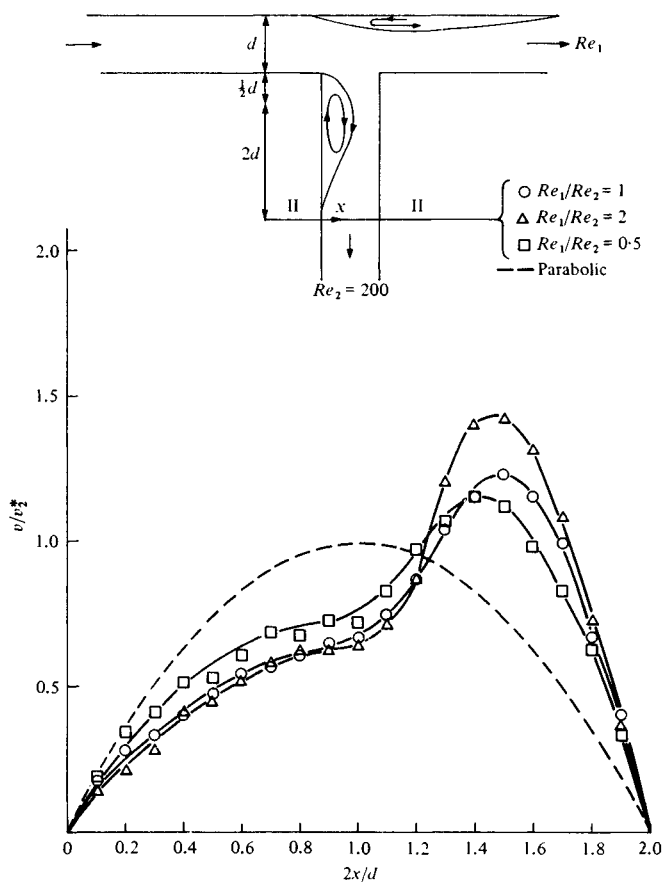


Fig. 5.15. Axial velocity profiles measured in the side-branch of a T-junction by N. Talukder & R. M. Nerem (personal communication). Re_1 , Re_2 are the Reynolds numbers in the daughter tubes: v_2^* is the average velocity in the branch. Details given in diagram.

relatively stagnant region. Talukder's measurements in unsteady flow show large-amplitude fluctuations in wall shear even in the 'stagnant' region (fig. 5.16). Note the peaks on the probe output associated with reversed shear; the probe response cannot be accurate near shear reversal (§ 3.1 and appendix), and whether it is accurate at other times depends on the probe characteristics (not described by Talukder (1975)).

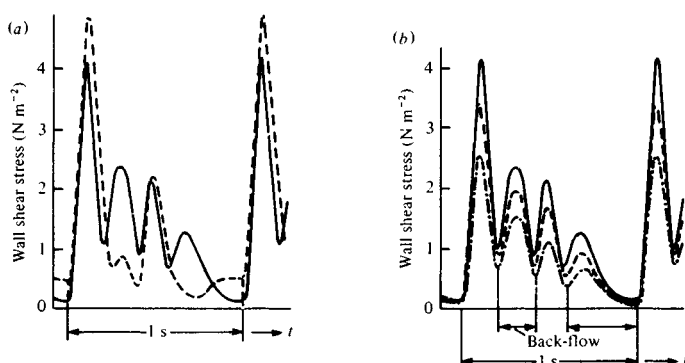


Fig. 5.16. Measurements of unsteady wall shear stress for asymmetric flow in a symmetric bifurcation; point of measurement is on the outer wall of the daughter tube containing the lower flow-rate, just downstream of the bifurcation (a region of separation in steady flow). (a) $\overline{Re}_0 = 500$; continuous curve, $\overline{Re}_2/\overline{Re}_1 = 0.43$; broken curve, $\overline{Re}_2/\overline{Re}_1 = 0.5$. (b) $\overline{Re}_2/\overline{Re}_1 = 0.43$; continuous curve, $\overline{Re}_0 = 500$; broken curve, $\overline{Re}_0 = 200$; dot-dash curve, $\overline{Re}_0 = 100$. \overline{Re}_0 , \overline{Re}_1 , \overline{Re}_2 are the mean Reynolds numbers in the parent tube and two daughter tubes, respectively. (After Talukder, 1975.)

Wall shear measurements have also been made, in a rigid cast of a canine descending aorta and its main branches, by Lutz *et al.* (1977) who used the electrochemical technique (§ 3.1). They made measurements in steady and unsteady flow at various sites on the ventral wall of the model aorta (approximately in the plane of symmetry) both upstream and downstream of the coeliac and superior mesenteric branches, but including sites actually in the bifurcation (fig. 5.17). Measurements were also made in the right renal branch, and at three positions round the circumference of the femoral artery. Typical results for steady flow are shown in fig. 5.17, and make it clear that the shear is low on the outside wall of a junction (inside of a bend) as at positions S_1 and S_3 in fig. 5.12, but is extremely high just downstream of a flow divider. This is to be expected both because new boundary layers are formed there and because high-velocity fluid is brought near to the flow divider by the splitting of the upstream flow. The effect is particularly pronounced here because the flow dividers protrude into the main stream (upper part of fig. 5.17(a)) and do not remain flush with the parent-tube wall (in this respect they resemble symmetric bifurcations); this

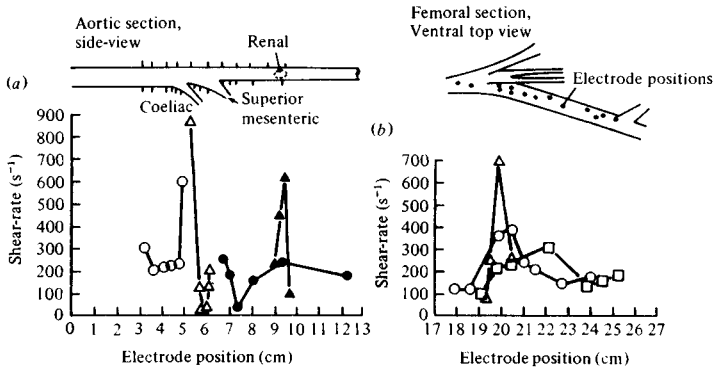


Fig. 5.17. Shear stress distribution pattern on ventral side of model artery in (a) aortic and (b) femoral sections. Electrode positions are indicated in the schematic drawing of the artery at the top of the figure. (a) Open circles, coeliac (flow-rate, $1.32 \text{ cm}^3 \text{ s}^{-1}$); open triangles, superior mesenteric (flow-rate, $2.57 \text{ cm}^3 \text{ s}^{-1}$); filled circles, abdominal aortic (flow-rate, $8.33 \text{ cm}^3 \text{ s}^{-1}$); filled triangles, renal (the right renal branch, which runs perpendicular to the plane of the figure; flow-rate, $1 \text{ cm}^3 \text{ s}^{-1}$). (b) In the femoral section, electrodes were placed on the inner wall (open triangles), centre line (open circles) and outer wall (open squares); flow-rate, $2.5 \text{ cm}^3 \text{ s}^{-1}$. (After Lutz *et al.*, 1977.)

protrusion probably also causes local separation, which is why the shear falls so rapidly downstream of the coeliac and superior mesenteric flow dividers. At higher flow-rates (greater than $12.5 \text{ cm}^3 \text{ s}^{-1}$) turbulent fluctuations in wall shear were observed, consistent with the presence of separated flow at large Reynolds number. The measurements in the femoral artery (fig. 5.17(b)) suggest that relatively high shear is maintained half-way round the circumference of the tube, just downstream of the flow divider, as in curved tubes (chapter 4). Lutz *et al.*'s results in unsteady flow confirm those of Talukder (1975), showing large-amplitude oscillations, especially in regions where the steady flow is separated. The main qualitative lessons to be learnt from the work of Lutz *et al.* are (a) that small irregularities in geometry do normally exist and have a marked effect on local wall shear, and (b) that changes in the relative flow-rates in different branches can completely alter the distribution of wall shear in the parent vessel (e.g. occlusion of the coeliac branch appears to abolish the separation downstream of the superior mesenteric branch). These conclusions

confirm the need for a detailed knowledge of local shear stress distribution before its effect on mass transport or arterial disease can be properly assessed.

5.2.2 *Effect of a weak branch on flow in the parent tube*

In this subsection and the next we describe the limited theoretical progress that has been made in analysing the flow through an asymmetric bifurcation in which a daughter tube branches at right angles off an otherwise straight parent. The theory summarised here enables the effect of the branch on the flow far upstream or downstream to be determined, while the next subsection presents a preliminary attempt at a detailed theory for the flow in the neighbourhood of a very small side-branch. The latter was intended as a model for flow into the intercostal arteries, but is unlikely to be quantitatively applicable because in order to allow progress the analysis was restricted to low-Reynolds-number flow in the side-branch.

Here we take a long straight parent tube of radius a_0 , and model the branch as an extended, $O(a_0)$, region of the wall over which the normal velocity is a given, steady function of position and is small compared with a typical axial velocity in the parent tube. If the axial and azimuthal velocities across the mouth of the branch are of the same order of magnitude as the normal velocity, they do not influence the solution to the order retained, and can therefore be set equal to zero. However, because this theory neglects these details of the motion across the branch, it cannot describe the local flow accurately; it is expected to give correct results sufficiently far from the branch. The analysis to be presented was given by Smith (1976c), who also applied it to non-symmetric deformation of the parent tube wall (with no branch), and to unsteady side-tube velocities (or unsteady deformations), but not to unsteady parent-tube flows.

We adopt cylindrical polar coordinates (a_0r, θ, a_0s) in the parent tube, with corresponding velocity components $\hat{W}_0(u, v, w)$ and pressure $\mu \hat{W}_0 p/a_0$, so that the governing parameter in the Navier-Stokes equations is the Reynolds number, $Re = \hat{W}_0 a_0/\nu$, which we take to be large. The mouth of the branch, B , is defined as the region $r = 1$, $0 < s < l$, $-\alpha(s) < \theta < \alpha(s)$, which determines the zero of the

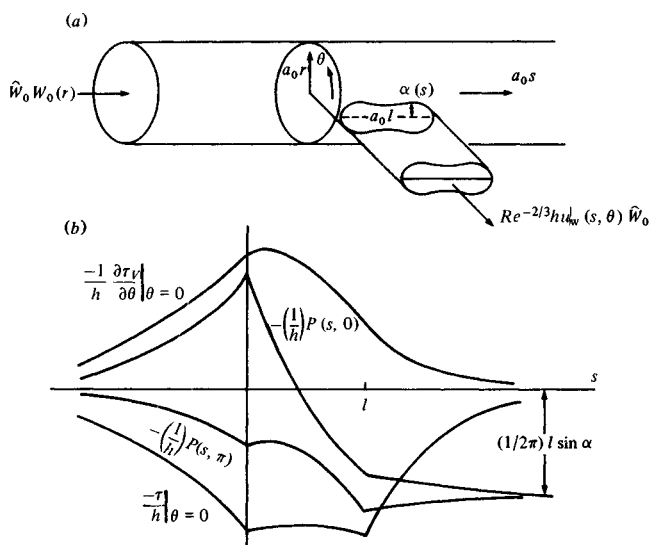


Fig. 5.18. (a) Coordinate system for flow in a side-branch. (b) Results of linearised theory, as described in text. (After Smith, 1976c.)

s -coordinate, and is taken to be symmetric about $\theta = 0$ (see fig. 5.18(a)). The boundary conditions on the velocity components are: on $r = 1$, $u = v = w = 0$ except in B , where $u = Re^{-2/3} h u_w(s, \theta)$ and h is a scale factor so that u_w is $O(1)$ for all h ; as $s \rightarrow -\infty$, $w \sim W_0(r) \equiv \frac{1}{4}(1 - r^2)$, $u \sim v \rightarrow 0$, $p \rightarrow p_0 - s$, where p_0 is a constant.

The upstream condition of Poiseuille flow is the same as that imposed in the curved-tube problem of § 4.5, so it should come as no surprise that the upstream adjustment of the flow, as it approaches the asymmetric disturbance, takes the same form as in that case, i.e. the core remains undisturbed, but there is a marked interaction in the boundary layer. Indeed, it is this consideration that suggested the $Re^{-2/3}$ scaling chosen above for the normal velocity into the branch. The theory proceeds for $Re \rightarrow \infty$ while s and h remain $O(1)$. As in the curved-tube case, the scaling suggests that there are $O(Re^{-1/3})$ perturbations to the Poiseuille flow in the core, but the inviscid equations of motion are satisfied to this order by a solution that is identically zero. The core perturbation is therefore only $O(Re^{-2/3})$, and we do not calculate it (although for a detailed examination of the flow near the branch we would have to

analyse perturbations of this order). In the boundary layer, however, perturbations of $O(Re^{-1/3})$ cannot be ruled out, and we write

$$\begin{aligned} u &= -Re^{-2/3}U(s, \zeta, \theta) + O(Re^{-1}), \\ v &= Re^{-1/3}V(s, \zeta, \theta) + O(Re^{-2/3}), \\ w &= Re^{-1/3}W(s, \zeta, \theta) + O(Re^{-2/3}), \\ p &= Re^{1/3}P(s, \theta) + O(1), \end{aligned} \quad (5.18)$$

where

$$\zeta = (1-r)Re^{1/3}$$

is the boundary layer coordinate, and P is independent of ζ from the radial momentum equation. The other governing equations are

$$\left. \begin{aligned} U_\zeta + V_\theta + W_s &= 0, \\ UV_\zeta + VV_\theta + WW_s &= -P_\theta + V_{\zeta\zeta}, \\ UW_\zeta + VW_\theta + WW_s &= -P_s + W_{\zeta\zeta}, \end{aligned} \right\} \quad (5.19)$$

with boundary conditions:

$$\left. \begin{aligned} \text{on } \zeta = 0, \quad V = W = 0, \quad U &= -hu_w(s, \theta) \text{ on } B, \\ &= 0 \text{ elsewhere,} \\ \text{as } \zeta \rightarrow \infty, \quad U_\zeta, V, (W - \tfrac{1}{2}\zeta) &\rightarrow 0, \\ \text{as } s \rightarrow -\infty, \quad U, V, P, (W - \tfrac{1}{2}\zeta) &\rightarrow 0. \end{aligned} \right\} \quad (5.20)$$

The use of the no-slip condition on B implies that v and w are expected to be $O(Re^{-2/3})$ there, which as explained above means that local details of the flow cannot be analysed to this order. There is no reason, however, apart from that of great labour, why the present analysis cannot be extended to the next order in $Re^{-1/3}$ and then the local details could be calculated if the distribution of v and w on B were known. In a real problem, of course, these distributions would not be known, and finding them would require a simultaneous solution of the problem in the side-tube (see § 5.2.3 below for a low-Reynolds-number example).

It is perhaps surprising that the relatively large pressure perturbation induced in the boundary layer should have negligible effect on the core flow. This is because the jet-like flow in the boundary layer is adequate to balance the induced pressure gradient. In an unbounded, external flow, or in a two-dimensional channel, on the

other hand, such pressure perturbations inevitably result in displacement of the primary flow (Stewartson, 1974; Smith 1976*d, e*).

Equations (5.19) are non-linear and, in general, require numerical solution (which has not been performed). However, the effect of the disturbance on the flow far upstream can be assessed by calculating the eigensolutions of the problem obtained by linearising about the oncoming Poiseuille flow. If we seek a solution of the form (as $s \rightarrow -\infty$)

$$\left. \begin{aligned} W &= \frac{1}{2}\zeta + e^{\kappa s} \cos m(\theta - \varepsilon)f(\zeta), \\ U &= e^{\kappa s} \cos m(\theta - \varepsilon)g(\zeta), \\ V &= e^{\kappa s} \sin m(\theta - \varepsilon)k(\zeta), \\ P &= b e^{\kappa s} \cos m(\theta - \varepsilon), \end{aligned} \right\} \quad (5.21)$$

where b , m , κ , ε are unknown constants (m is an integer), the equations reduce to

$$\begin{aligned} \kappa f + g' + mk &= 0, \\ \frac{1}{2}\zeta \kappa k &= mb + k'', \\ \frac{1}{2}\zeta \kappa f + \frac{1}{2}g &= -\kappa b + f''. \end{aligned}$$

The functions f , g and k are to be zero at $\zeta = 0$ and f , g' , k must be zero as $\zeta \rightarrow \infty$. The problem is now virtually the same as that already solved in § 4.5, and solution in the same way leads to the conclusions that $\kappa = m$, that $g \equiv 0$ and that

$$f = -k = [bm^{1/3}/(\frac{1}{2})^{2/3}]L(t),$$

where $t = (\frac{1}{2}m)^{1/3}\zeta$ and $L(t)$ is defined by (4.102). The constants b , m , ε remain undetermined. In general the solution will be the sum over all positive integers m of terms like (5.21), with $\kappa = m$ and b , ε depending on m ; the values of b and ε in each term can be fixed only after solution for all values of s . The term to persist furthest upstream will be that with $m = 1$, and this will describe the maximum upstream response in any asymmetrically disturbed pipe flow (cf. p. 226).

In the absence of a numerical solution to the non-linear equations (5.19), detailed calculations can be made only for problems that can be linearised for all s of $O(1)$, i.e. for which $h \ll 1$. The problem once

more becomes virtually the same as that defined by (4.98). We therefore write

$$W = \frac{1}{2}\zeta + h\bar{W}, \quad (U, V, P) = h(\bar{U}, \bar{V}, \bar{P}),$$

retain only terms of $O(h)$ in (5.19), take Fourier transforms in s (defined by (4.100) and again denoted by $\tilde{P}(\omega, \theta)$ etc.), solve the resulting inhomogeneous Airy equations as in (4.102–3), and apply the boundary conditions derived from (5.20). The conditions at infinity show that $\tilde{B}(\omega, \theta)$, a term exactly analogous to the function $\tilde{B}(\omega)$ introduced in (4.103), is given by

$$\tilde{B} = [\tilde{P}_{\theta\theta}/6Ai^2(0)](0 + \frac{1}{2}i\omega)^{-5/3}.$$

The boundary condition at $\zeta = 0$ then gives

$$(1/i\omega)\tilde{P}_{\theta\theta} + i\omega\tilde{P} = \frac{1}{2}\tilde{u}_w(\omega, \theta),$$

where \tilde{u}_w is the Fourier transform of the normal velocity into the branch. If we now Fourier analyse in the θ -direction also, writing

$$[\tilde{u}_w, \tilde{P}](\omega, \theta) = \sum_{m=0}^{\infty} [\tilde{u}_{wm}(\omega), \tilde{P}_m(\omega)] \cos m\theta$$

since the branch (and by inference the flow into it) is symmetric about $\theta = 0$, we obtain

$$\tilde{P}_m = \frac{1}{2}\tilde{u}_{wm}/(i\omega - m^2/i\omega). \quad (5.22)$$

From this result all quantities of interest are derived.

Smith (1976*c*) worked out the detailed results for a simple case, in which the mouth B of the branch had rectangular cross-section ($0 < s < l, -\alpha < \theta < \alpha$; α constant) and the component of velocity through it parallel to the axis of the branch (supposed to be at right angles to the axis of the parent tube) was uniform, i.e. $u_w = \cos \theta$ in B . Hence

$$\tilde{u}_{wm}(\omega) = (A_m/i\omega)(1 - e^{-i\omega l}),$$

where

$$\pi A_0 = \sin \alpha, \quad 2\pi A_1 = 2\alpha + \sin 2\alpha,$$

$$(m^2 - 1)\pi A_m = 2(m \sin m\alpha \cos \alpha - \cos m\alpha \sin \alpha) \text{ for } m \geq 2.$$

Inverting (5.22) we have

$$P(s, \theta) = h \left[\frac{1}{2}A_0 s H(s) - \frac{1}{4} \sum_{m=1}^{\infty} \frac{A_m}{m} e^{-m|s|} \cos m\theta \right] \quad (5.23)$$

minus a similar term with $s - l$ for s . The corresponding expressions for the perturbation to the axial wall shear, τ , and for the azimuthal wall shear, τ_v , are

$$\begin{aligned} \frac{\tau}{h} &= \frac{(\frac{1}{2})^{2/3}}{6Ai(0)} \sum_{m=1}^{\infty} e^{ms} m^{-1/3} A_m \cos m\theta \quad \text{for } s < 0 \\ &= \frac{-(\frac{1}{2})^{2/3}}{3Ai(0)} \sum_{m=1}^{\infty} \frac{A_m \cos m\theta}{m^{1/3}} \left[\frac{e^{-ms}}{4} - \frac{3\sqrt{3}}{2\pi} \Gamma(\frac{2}{3})(ms)^{1/3} \right. \\ &\quad \left. + \frac{\sqrt{3}}{2\pi} \int_0^{\infty} \frac{\xi^{2/3} e^{-ms\xi}}{1-\xi^2} d\xi \right] \quad \text{for } s > 0 \end{aligned} \quad (5.24)$$

and

$$\begin{aligned} \frac{\tau_v}{h} &= \frac{-(\frac{1}{2})^{2/3}}{6Ai(0)} \sum_{m=1}^{\infty} e^{ms} m^{-1/3} A_m \sin m\theta \quad \text{for } s < 0 \\ &= \frac{-(\frac{1}{2})^{2/3}}{3Ai(0)} \sum_{m=1}^{\infty} \frac{A_m \sin m\theta}{m^{1/3}} \left[\frac{e^{-ms}}{4} \right. \\ &\quad \left. + \frac{\sqrt{3}}{2\pi} \int_0^{\infty} \frac{\xi^{-1/3} e^{-ms\xi}}{1-\xi^2} d\xi \right] \quad \text{for } s > 0, \end{aligned} \quad (5.25)$$

again with similar expressions, containing $s - l$ for s , to be subtracted. The negatives of these quantities are plotted against s in fig. 5.18(b); the figure is taken from Smith's paper, and the negative sign comes from the fact that he was considering injection into the parent tube, which may be relevant to flow in veins. The curve of $-(1/h)P(s, \pi)$ against s shows that the net pressure rise (relative to the linearly falling Poiseuille pressure drop) is independent of θ . The curves of $-(1/h)P(s, 0)$, and of $-\tau/h$ and $-(1/h)\partial\tau_v/\partial\theta$ evaluated on $\theta = 0$, show that, on $\theta = 0$, the pressure falls and the axial shear rises ahead of the branch, while over the mouth of the branch itself the pressure rises sharply; downstream, the pressure perturbation continues to rise slowly to its asymptotic value, while the axial shear perturbation falls again to zero. On $\theta = \pi$ there is a pressure rise and a shear fall in the neighbourhood of the branch; it is these features that, when the outflow is stronger, lead to separation (S_2 in fig. 5.12). It is possible that such three-dimensional separation upstream of the branch could be described in a regular way by the non-linear equations (5.19) even when the outflow is too

strong for the theory to be valid in the neighbourhood of the branch (as in the two-dimensional case (Smith, 1976*d*)). The azimuthal shear curve indicates that the secondary motion in the boundary layer is everywhere directed towards $\theta = 0$ (where the branch is), consistent with the excess pressure everywhere at $\theta = \pi$. As in the case of flow into a curve that subsequently straightens out without net change of direction, the solution breaks down when $s = O(Re)$, but the perturbation is by then very small anyway.

Another example that is relevant to the effect on the parent tube of a very small branch is that in which $u_w = \delta(\theta)\delta(s)$. In this case, $\tilde{u}_{wm} = 1/\pi$ for all m , and

$$\tilde{P}_m = \frac{1/2\pi}{i\omega - m^2/i\omega}. \quad (5.23a)$$

Inverting the various Fourier transforms gives:

$$\frac{P}{h} = \frac{1}{2\pi} \left[H(s) + \sum_{m=1}^{\infty} \frac{1}{2} e^{-m|s|} \cos m\theta \operatorname{sgn} s \right] \quad \text{for all } s; \quad (5.26)$$

$$\begin{aligned} \frac{\tau}{h} &= \frac{1}{2\pi \cdot 3Ai(0)} \sum_{m=1}^{\infty} (\tfrac{1}{2}m)^{2/3} e^{ms} \cos m\theta \quad \text{for } s < 0, \\ &= \frac{1}{\pi \cdot 3Ai(0)} \sum_{m=1}^{\infty} (\tfrac{1}{2}m)^{2/3} \cos m\theta \left[\frac{\sqrt{3}}{2\pi} \Gamma(\tfrac{2}{3})(ms)^{-2/3} + \frac{e^{-ms}}{4} \right. \\ &\quad \left. + \frac{\sqrt{3}}{2\pi} \int_0^{\infty} \frac{e^{-ms\xi} \xi^{5/3}}{1 - \xi^2} d\xi \right] \quad \text{for } s > 0; \end{aligned} \quad (5.27)$$

$$\begin{aligned} \frac{\tau_v}{h} &= \frac{-1}{2\pi \cdot 3Ai(0)} \sum_{m=1}^{\infty} (\tfrac{1}{2}m)^{2/3} e^{ms} \sin m\theta \quad \text{for } s < 0, \\ &= \frac{1}{\pi \cdot 3Ai(0)} \sum_{m=1}^{\infty} (\tfrac{1}{2}m)^{2/3} \sin m\theta \\ &\quad \times \left[\frac{e^{-ms}}{4} + \frac{\sqrt{3}}{2\pi} \int_0^{\infty} \frac{e^{-ms\xi} \xi^{2/3}}{1 - \xi^2} d\xi \right] \quad \text{for } s > 0. \end{aligned} \quad (5.28)$$

The interesting features of this solution are the step rise in pressure everywhere within the boundary layer across $s = 0$, corresponding to the more gradual rise of fig. 5.18(*b*), and the leading term in the

axial wall shear expansion for $s > 0$. The first term in the square brackets of (5.27) is, in fact, independent of m , so the axial shear has a term proportional to $s^{-2/3}[\delta(\theta) - \frac{1}{2}]$, which means that, in practice, the presence of a branch has a strong influence on the axial wall shear in a narrow band exactly downstream of the mouth of the branch. This is reminiscent of the 'corridor' downstream of a three-dimensional hump in a two-dimensional boundary layer, predicted both by Smith, Sykes & Brighton (1977), for the case where the horizontal length-scale of the hump is much greater than the boundary layer thickness, and by Brighton (1977) for the case where it is comparable with the boundary layer thickness. The wake of the side-hole will be examined in more detail in the next subsection. This wake may indeed be relevant to the observations of Cornhill & Roach (1976), reported in § 1.2.6, that the development of atheroma around the mouths of the intercostal arteries in cholesterol-fed rabbits varies from one pair of intercostals to the next. The present theory suggests that, if a second branch is directly in the wake of the first, the wall shear in the neighbourhood of the second will be modified.

The present theory, especially this last example, clearly exhibits singular behaviour near $s = 0$, and more terms in the Navier–Stokes equations must be taken into account in order to smooth them out and describe the detailed motion near the mouth of the branch. The next subsection represents an approach to the complete solution in a particular case.

5.2.3 *Flow into a very small, very weak branch*

Here we examine the details of the flow into a small side-branch in which the flow is so slow that it is inertia-free and satisfies the Stokes equations. This is clearly a far cry from large aortic branches, but it is the only case in which an attempt has been made to analyse the complete flow, including the effect of the velocities across the mouth of the tube as well as the normal velocity into it. The perturbation to the basic flow is so weak that the pressure perturbation in the $O(Re^{-1/3})$ boundary layer, which was central to the solutions of the last subsection, is $o(Re^{1/3})$ and therefore negligible to that order of magnitude. Thus the boundedness of the flow is irrelevant, and we can suppose the side-hole to be embedded in a plane wall. This

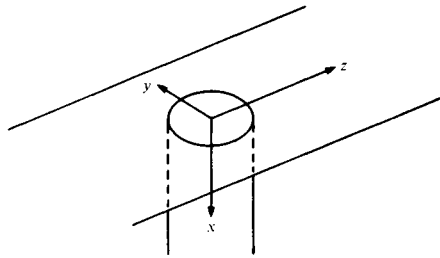


Fig. 5.19. Coordinate system for flow in a small side-branch.

problem has been formulated, and its solution outlined, by Sobey (1976*b*).

The geometry is shown in fig. 5.19. The side-tube is a cylinder of radius $b = \delta a_0$ ($\delta \ll 1$), coming off the parent tube (radius a_0) at right angles; the Reynolds number $Re = \hat{W}_0 a_0 / \nu$ of the parent-tube flow is still taken to be large. Let the flow-rate in the side-tube be \hat{Q} , and define $q = \hat{Q} a_0 / \hat{W}_0 b^3$. Using coordinates $b(x, y, z)$, where x is measured down the side-tube axis, z is the longitudinal coordinate in the parent tube, and y is at right angles to both, we define velocity components as follows (as usual, $\hat{\cdot}$ denotes a dimensional quantity).

In $x < 0$ (the parent tube)

$$(\hat{u}, \hat{v}) = \hat{W}_0 \delta q(u, v),$$

$$\hat{w} = \hat{W}_0 [\tilde{W}(-\delta x) + \delta q w],$$

where (u, v, w) depend on (x, y, z) , and

$$\tilde{W}(\xi) = \frac{1}{4}(2\xi - \xi^2)$$

is the basic Poiseuille flow in the parent tube. In $x > 0$ (the side-tube)

$$(\hat{v}, \hat{w}) = \hat{W}_0 \delta q(v', w'),$$

$$\hat{u} = \hat{W}_0 \delta q[(2/\pi)(1 - y^2 - z^2) + u'],$$

where u' is the perturbation to the Poiseuille flow that develops for large values of x . We define pressures

$$P_0 + \rho \hat{W}_0^2 Re^{-1} (-\delta z + qp) \quad \text{in } x < 0,$$

$$\rho \hat{W}_0^2 Re^{-1} q[-(8/\pi)x + p'] \quad \text{in } x > 0.$$

The governing equations in $x < 0$ are therefore

$$\begin{aligned} u_x + v_y + w_z &= 0, \\ \nabla^2 u - p_x &= \delta Re \tilde{W}(-\delta x) u_z + \delta^2 Req(uu_x + vu_y + wu_z), \\ \nabla^2 v - p_y &= \delta Re \tilde{W}(-\delta x) v_z + \delta^2 Req(uv_x + vv_y + wv_z), \\ \nabla^2 w - p_z &= \delta Re [\tilde{W}(-\delta x) w_z - \delta \tilde{W}'(-\delta x) u] \\ &\quad + \delta^2 Req(uw_x + vw_y + ww_z), \end{aligned} \quad (5.29)$$

while in $x > 0$ they are

$$\nabla^2 \mathbf{u}' - \nabla p' = O(\delta^2 Req), \quad (5.30)$$

where $\mathbf{u}' = (u', v', w')$. The boundary conditions are

$$\begin{aligned} u = v = w &= 0 \quad \text{on } x = 0, \quad y^2 + z^2 > 1, \\ u, v, w &\rightarrow 0 \quad \text{as } (x^2 + y^2 + z^2) \rightarrow \infty, \quad x \leq 0, \\ u' = v' = w' &= 0 \quad \text{on } y^2 + z^2 = 1, \quad x > 0, \\ u', v', w' &\rightarrow 0 \quad \text{as } x \rightarrow \infty, \end{aligned}$$

together with the condition that all velocity and stress components must be continuous at the mouth of the hole. That is,

$$\begin{aligned} \{u, v, w, p - (\delta/q)z, v_x, -[\tilde{W}'(0)/q] + w_x\} \\ = \{u' + (2/\pi)(1 - y^2 - z^2), v', w', p', v'_x, w'_x\} \end{aligned} \quad (5.31)$$

on $x = 0$, $y^2 + z^2 < 1$.

Since $\tilde{W}(-\delta x) = O(\delta)$ when $x = O(1)$, the right-hand side of (5.29) is $O(\delta^2 Re)$ for $x = O(1)$, and to make progress we suppose that $\delta Re^{1/2} \ll 1$, while q remains $O(1)$: note that q is the ratio of a typical shear-rate in the side-tube to that in the parent, and that $\delta^2 Req$ is the Reynolds number of the side-tube flow. In the region $|\mathbf{x}| = O(1)$ the equations reduce, to leading order, to Stokes's equations

$$\nabla^2(\mathbf{u}, \mathbf{u}') = \nabla(p, p'), \quad \nabla \cdot (\mathbf{u}, \mathbf{u}') = 0$$

and the primary velocity field in the parent tube enters the problem only through its contribution to the shear stress boundary condition in (5.31). The Stokes flow problem has a single dimensionless parameter in it, $\tilde{W}'(0)/q$; this equals $\frac{1}{2}q$ for the case of Poiseuille flow in the parent tube (the same theory can be set out for other distributions of parent-tube flow). For a given value of this

parameter, the Stokes flow problem can, in principle, be solved as follows: (a) guess distributions of u , v , w over the mouth of the tube, say

$$u = U(y, z), \quad v = V(y, z), \quad w = W(y, z); \quad (5.32)$$

(b) calculate the two Stokes flows, in $x < 0$ and $x > 0$, corresponding to these velocity distributions; (c) compute the pressure and shear stresses at $x = 0^-$ and $x = 0^+$, and equate them. This should result in three simultaneous integral equations for U , V , W that must be solved iteratively. In fact, unless there is a simple analytical form for the solutions in both $x < 0$ and $x > 0$, it will probably be simpler to solve the finite-difference form of Stokes's equations by direct numerical integration. Sobey (1977) found this to be true in the two-dimensional version of this problem (despite the existence of a simple solution in $x < 0$), but he has not yet embarked on the more difficult three-dimensional numerical problem. The solution in the present case is therefore still incomplete.

Nevertheless, it is useful to examine the nature of the solution in $x < 0$, in order to see how the wall shear in the parent tube is affected by the presence of the side-branch. Sobey (1976*b*) pointed out that the Stokes flow problem is a familiar one in elasticity theory (Sokolnikoff, 1956), and that the solution in $x < 0$ corresponding to the velocity distribution (5.32) at the mouth of the side-branch (B) can be constructed as the sum of three integrals over B . The integrand in each is the velocity distribution at B times the velocity field due to a particular kind of singularity at a particular point (y_0, z_0) of B . The three singularities are

$$(a) \quad v = w = 0, \quad u = \delta(y - y_0)\delta(z - z_0) \quad \text{on } x = 0,$$

$$(b) \quad u = w = 0, \quad v = \delta(y - y_0)\delta(z - z_0) \quad \text{on } x = 0,$$

$$(c) \quad u = v = 0, \quad w = \delta(y - y_0)\delta(z - z_0) \quad \text{on } x = 0.$$

Using Fourier transforms over the (y, z) -plane, Sobey showed that the velocity and pressure fields in each case are:

$$\begin{aligned} (a) \quad u &= -3x^3/2\pi\rho_0^5, & v &= -3x^2(y - y_0)/2\pi\rho_0^5, \\ w &= -3x^2(z - z_0)/2\pi\rho_0^5, & p &= -(3/2\pi)(2x^2/\rho_0^5 - 2/3\rho_0^3), \end{aligned} \quad (5.33a)$$

where $\rho_0^2 = x^2 + (y - y_0)^2 + (z - z_0)^2$;

$$\begin{aligned}
 (b) \quad u &= -3x^2(y - y_0)/2\pi\rho_0^5, & v &= -3x(y - y_0)^2/2\pi\rho_0^5, \\
 w &= -3x(y - y_0)(z - z_0)/2\pi\rho_0^5, & p &= -3x(y - y_0)/\pi\rho_0^5;
 \end{aligned}
 \tag{5.33b}$$

$$\begin{aligned}
 (c) \quad u &= -3x^2(z - z_0)/2\pi\rho_0^5, & v &= -3x(y - y_0)(z - z_0)/2\pi\rho_0^5, \\
 w &= -3x(z - z_0)^2/2\pi\rho_0^5, & p &= -3x(z - z_0)/\pi\rho_0^5.
 \end{aligned}
 \tag{5.33c}$$

The shear on the wall $x = 0$, a vector in the (y, z) -plane, is proportional to $\tau = [-v_x, -w_x]_{x=0}$, and is therefore given by

$$\begin{aligned}
 \tau &= \frac{3}{2\pi} \iint_B [V(y_0, z_0)(y - y_0) + W(y_0, z_0)(z - z_0)] \\
 &\quad \times [y - y_0, z - z_0] \rho_0^{-5} dy_0 dz_0
 \end{aligned}
 \tag{5.34}$$

for $(y, z) \notin B$. This result will be true for any shape B of the mouth of the side-branch.

The most striking aspect of the result (5.34) is that it is independent of the distribution of normal velocity U into the side-branch; only the velocities *across* the mouth affect the wall shear in the region of Stokes flow. This means that any theory, such as that of Smith (1976c), which was presented in § 5.2.2 and which represents a branch by its distribution of normal velocity alone, cannot give a correct prediction of wall shear near the branch (if inertia is locally negligible). Of course, the flow-rate into the side-tube will affect the shear distribution because, through the parameter q , it enters the boundary conditions (5.31) that determine the functions $V(y_0, z_0)$, $W(y_0, z_0)$.

For large values of $\rho = (y^2 + z^2)^{1/2}$, the wall shear (5.34) can be expanded as follows:

$$\begin{aligned}
 \tau &= (3[y, z]/2\pi\rho^5)\{yK_V + zK_W - K_{V1} - K_{W2} \\
 &\quad + (5/\rho^2)[y^2K_{V1} + yz(K_{V2} + K_{W1}) + z^2K_{W2}]\} \\
 &\quad - (3/2\pi\rho^5)[yK_{V1} + zK_{W1}, yK_{V2} + zK_{W2}] + O(\rho^{-5}),
 \end{aligned}$$

where

$$K_{V,W} = \iint_B [V(y_0, z_0), W(y_0, z_0)] dy_0 dz_0, \quad (5.35)$$

$$K_{V1,2} = \iint V(y_0, z_0)[y_0, z_0] dy_0 dz_0,$$

and similarly for $K_{W1,2}$. In cases with symmetry about the plane $y = 0$, V will be an odd function of y_0 , and W an even function of y_0 , so that $K_V = K_{V2} = K_{W1} = 0$. In this case the leading term in the far field depends only on $W(y_0, z_0)$, since

$$\tau = (3/2\pi)[y, z](zK_W/\rho^5) + O(\rho^{-4}), \quad (5.36)$$

and the distribution $V(y_0, z_0)$ of lateral velocity across the mouth of the hole is important only at the next order (through K_{V1}).

The Stokes flow solution in $x < 0$ breaks down where the neglected terms in (5.29) become $O(1)$. This occurs where

$$r = (x^2 + y^2 + z^2)^{1/2} = O(\delta^{-1}Re^{-1/2}) \gg 1,$$

which is equivalent to a dimensional distance \hat{r} from the origin, where $\hat{r}/a_0 = O(Re^{-1/2}) \ll 1$. Thus the region where the Stokes flow breaks down is still very near the hole on the length-scale of the parent-tube radius, but is far from it on the length-scale of the side-tube radius. At this distance from the origin, the velocity perturbations (u, v, w) are $O(r^{-2})$ from (5.33), which is $O(\delta^2 Re) \ll 1$. Thus in this region we rescale the variables according to

$$\tilde{\mathbf{x}} = \delta Re^{1/2} \mathbf{x} = Re^{1/2} \hat{\mathbf{x}}/a_0, \quad \tilde{\mathbf{u}} = \delta^{-2} Re^{-1} \mathbf{u}, \quad \tilde{p} = \delta^{-3} Re^{-3/2} p,$$

and, noting that $\tilde{W}(-\delta x) = \tilde{W}(-Re^{-1/2} \tilde{x})$, we obtain from (5.29) (for $x < 0$ only)

$$\left. \begin{aligned} \tilde{u}_{\tilde{x}} + \tilde{v}_{\tilde{y}} + \tilde{w}_{\tilde{z}} &= 0, \\ \nabla^2 \tilde{u} - \tilde{p}_{\tilde{x}} &= [-\tfrac{1}{2}\tilde{x} - \tfrac{1}{4}Re^{-1/2}\tilde{x}^2]\tilde{u}_{\tilde{z}} + O(\delta^3 Re^{3/2}q), \\ \nabla^2 \tilde{v} - \tilde{p}_{\tilde{y}} &= [-\tfrac{1}{2}\tilde{x} - \tfrac{1}{4}Re^{-1/2}\tilde{x}^2]\tilde{v}_{\tilde{z}} + O(\delta^3 Re^{3/2}q), \\ \nabla^2 \tilde{w} - \tilde{p}_{\tilde{z}} &= [-\tfrac{1}{2}\tilde{x} - \tfrac{1}{4}Re^{-1/2}\tilde{x}^2]\tilde{w}_{\tilde{z}} - \tfrac{1}{2}[1 - Re^{-1/2}\tilde{x}]\tilde{u} \\ &\quad + O(\delta^3 Re^{3/2}q). \end{aligned} \right\} \quad (5.37)$$

With $q = O(1)$ the non-linear terms remain negligible, and with $Re \gg 1$ so does the second term in each square bracket. The

boundary conditions are that $\tilde{\mathbf{u}} \rightarrow 0$ as $|\tilde{\mathbf{x}}| \rightarrow \infty$ and that $\tilde{\mathbf{u}} = 0$ on $\tilde{x} = 0$ except at the mouth of the side-branch. In the present scaling this is equivalent to

$$\tilde{\mathbf{u}} = (1, K_V, K_W)\delta(\tilde{y})\delta(\tilde{z}) \quad \text{on } \tilde{x} = 0, \quad (5.38)$$

where K_V, K_W are defined by (5.35) and $K_V = 0$ for a symmetrical flow. Since the problem is still linear its solution should incorporate the far-field of the Stokes flow, constructed from (5.33), as $|\tilde{\mathbf{x}}| \rightarrow 0$.

We may note that if near the wall but far from the hole the boundary layer approximation can be made, so that $\partial/\partial\tilde{y}$ and $\partial/\partial\tilde{z}$ are small compared with $\partial/\partial\tilde{x}$, the problem reduces to that considered at the end of the previous subsection, apart from the presence of K_V and K_W in (5.38). However the scaling of § 5.2.2 suggests that, if K_V and K_W are $O(1)$, they have no effect (to leading order) on the boundary layer solution. This would mean that the solution of the present problem should tend to that given by (5.26)–(5.28) as $(\tilde{y}^2 + \tilde{z}^2)^{1/2} \rightarrow \infty$, with the exception of those features, such as the step rise in pressure, that are a direct consequence of the confined geometry of the pipe and do not appear on the present much smaller length-scale for which the wall is represented as an unbounded plane. A useful check on both solutions would be to verify this conclusion.

The problem defined by the $O(1)$ terms of (5.37) and (5.38) can also be solved using Fourier transforms in \tilde{y} and \tilde{z} . We follow Sobey (1976*b*) and examine only the case $K_V = 0$. Defining

$$\tilde{f}(\tilde{x}, l, m) = \int_{-\infty}^{\infty} \int_{-\infty}^{\infty} e^{-im\tilde{y} - il\tilde{z}} f(\tilde{x}, \tilde{y}, \tilde{z}) \, d\tilde{y} \, d\tilde{z},$$

we obtain

$$(D^2 + \tfrac{1}{2}l\tilde{x})D^2\tilde{u} = 0,$$

where

$$D^2 = d^2/d\tilde{x}^2 - k^2 \quad \text{and} \quad k^2 = l^2 + m^2,$$

which must be solved subject to

$$\tilde{u}(0, l, m) = 1, \quad \tilde{u}(\tilde{x}, l, m) \quad \text{bounded as } \tilde{x} \rightarrow -\infty.$$

This has solution

$$\tilde{u} = [1 - \alpha S(0)] e^{-k\xi} + \alpha S(\xi), \quad (5.39)$$

where $\xi = -\tilde{x}$, α is an arbitrary constant, and $S(\xi)$ is defined by

$$S(\xi) = \int_{\xi}^{\infty} \frac{\sinh k(\xi - \xi')}{k} Ai[\zeta(\xi')] d\xi',$$

where

$$\zeta(\xi) = (0 + \frac{1}{2}il)^{1/3}(\xi + k^2/\frac{1}{2}il). \quad (5.40)$$

The third of equations (5.37), together with the boundary condition (5.38) with $K_V = 0$, yields the following expression for \bar{v} in terms of \bar{p} :

$$\begin{aligned} \bar{v}(\xi) = & \frac{im\pi}{(0 + \frac{1}{2}il)^{1/3}} \left\{ \frac{Bi(\gamma)}{Ai(\gamma)} Ai[\zeta(\xi)] \int_0^{\infty} Ai[\zeta(\xi')] \bar{p}(\xi') d\xi' \right. \\ & - Ai[\zeta(\xi)] \int_0^{\xi} Bi[\zeta(\xi')] \bar{p}(\xi') d\xi' \\ & \left. - Bi[\zeta(\xi)] \int_{\xi}^{\infty} Ai[\zeta(\xi')] \bar{p}(\xi') d\xi' \right\}, \end{aligned}$$

where the (l, m) -dependence of \bar{v} and \bar{p} is omitted, and

$$\gamma = \zeta(0) = (0 + \frac{1}{2}il)^{-2/3} k^2. \quad (5.41)$$

The continuity equation can now be used to derive \bar{w} , and α is then determined by the condition that \bar{w} satisfies the boundary condition (5.38), as follows:

$$\alpha = [k + ilK_W]/[S'(0) + kS(0)]. \quad (5.42)$$

Finally, substitution of \bar{w} and \bar{u} into the last of equations (5.37) gives the transform of the pressure:

$$\begin{aligned} \bar{p}(\xi) = & (-\frac{1}{2}il/k^2) \{ [1 - \alpha S(0)](1 + k\xi) e^{-k\xi} \\ & + \alpha [S(\xi) - \xi S'(\xi)] \} + \alpha Ai'[\zeta(\xi)](0 + \frac{1}{2}il)^{1/3}/k^2. \end{aligned} \quad (5.43)$$

The particular quantities of interest are the pressure on the wall, proportional to $p(\xi = 0)$, and the perturbations to the shear on the wall, proportional to $[v_{\xi}, w_{\xi}]_{\xi=0}$. Their transforms are given by

$$\left. \begin{aligned} \bar{p}|_{\xi=0} &= [\alpha Ai'(\gamma)(0 + \frac{1}{2}il)^{1/3} - \frac{1}{2}il]/k^2, \\ \bar{\tau}_v &= \bar{v}_{\xi}|_{\xi=0} = -im\bar{P}/Ai(\gamma), \\ \bar{\tau} &= \bar{w}_{\xi}|_{\xi=0} = (1/il)[k^2 - \alpha Ai(\gamma) - im\bar{\tau}_v], \end{aligned} \right\} \quad (5.44)$$

where

$$\bar{P}(l, m) = \int_0^\infty Ai[\zeta(\xi')] \bar{p}(\xi') d\xi'.$$

Substitution of (5.43) into this integral, followed by further manipulation, leads to the following expression for \bar{P} in terms of integrals whose asymptotic expansions (at least) can be deduced:

$$\begin{aligned} \bar{P} = & Ai(\gamma) - (\alpha/k^2) Ai^2(\gamma) - (2K_w/k^2)(0 + \tfrac{1}{2}il)^{4/3} Ai'(\gamma) \\ & - (il/4k^2)\{I_+(\gamma) + I_-(\gamma) + (ilK_w/k)[I_+(\gamma) - I_-(\gamma)] + 2\alpha I\}. \end{aligned} \quad (5.45)$$

In this equation

$$\begin{aligned} I_\pm(\xi) = & \int_0^\infty e^{\pm k\xi'} Ai[(0 + \tfrac{1}{2}il)^{1/3}\xi' + \xi] d\xi' \\ = & (0 + \tfrac{1}{2}il)^{-1/3} \exp[\mp(0 + \tfrac{1}{2}il)^{-1/3}k\xi] \\ & \times \int_\xi^\infty \exp[i(\pi/6)\operatorname{sgn} l] \exp[\pm k(0 + \tfrac{1}{2}il)^{-1/3}\zeta] Ai(\zeta) d\zeta \end{aligned} \quad (5.46)$$

and

$$\begin{aligned} I &= \int_0^\infty S(\xi) Ai[\zeta(\xi)] d\xi \\ &= J_+ + J_-, \end{aligned} \quad (5.47)$$

where

$$J_\pm = \frac{-(0 + \tfrac{1}{2}il)^{-1/3}}{2k} \int_\gamma^\infty \exp[i(\pi/6)\operatorname{sgn} l] I_\pm(\zeta) Ai(\zeta) d\zeta. \quad (5.48)$$

Note too that α (see (5.42)) is equal to $(k + ilK_w)/I_-(\gamma)$.

Numerical inversion of the above Fourier transforms has not yet been performed, and the only analysis concerns the asymptotic behaviour as

$$\rho = (\tilde{y}^2 + \tilde{z}^2)^{1/2} \rightarrow \infty \quad \text{and} \quad \rho \rightarrow 0.$$

The corresponding two-dimensional problem has been fully investigated by Sobey (1976*b*, 1977), and in addition to his numerical results he showed that the solution does match with the Stokes flow as $|\tilde{z}| \rightarrow 0$ and with the appropriate small- $|\tilde{z}|$ expansion of the boundary layer solution (Smith, 1974; Brighton, 1977) as

$|\tilde{z}| \rightarrow \infty$. The results given on p. 276 indicate that in the present, three-dimensional problem one should expect a different structure to the flow in the wake of the hole from that elsewhere. Thus the asymptotic form of the solution at large distances from the hole will depend on whether or not $|\tilde{y}| \rightarrow \infty$ as $\rho \rightarrow \infty$.

Wall pressure and shear far from the hole: $\rho \rightarrow \infty$, $|\tilde{y}| \rightarrow \infty$

In order to obtain the leading terms describing the flow when both $|\tilde{z}|$ and $|\tilde{y}|$ are large, we must take the leading terms of (5.44) as both l and m (and hence also k) tend to zero together. In this case $|\gamma| \ll 1$, and asymptotic analysis of the integrals in (5.46) and (5.48) shows that $I_{\pm}(\gamma) = O(|l|^{-1/3})$, $I = O(|l|^{-1})$; the leading term in \bar{P} turns out to be that involving $[I_+(\gamma) + I_-(\gamma)]$. In the limit, the three quantities given in (5.44) become

$$\left. \begin{aligned} \bar{p}|_{\xi=0} &\sim -il/2k^2, \\ [\bar{\tau}_v, \bar{\tau}] &\sim [-l, m][m(0 + \frac{1}{2}il)^{-1/3}/6Ai(0)k^2], \end{aligned} \right\} \quad (5.49)$$

and inverting them gives

$$p|_{\xi=0} \sim \sin \Theta / 4\pi\rho, \quad (5.50)$$

$$\left. \begin{aligned} \tau_v &\sim \frac{-2^{1/3}\Gamma(\frac{2}{3})}{18\pi Ai(0)\rho^{5/3}} \cos(\frac{5}{3}\Theta + \frac{1}{3}\pi) \operatorname{sgn} \tilde{y}, \\ \tau &\sim \frac{\Gamma(\frac{2}{3})}{6\pi Ai(0)} \left[\frac{\sqrt{3}}{2|\tilde{z}|^{2/3}} H(\tilde{z}) \delta(\tilde{y}) - \frac{2^{1/3} \sin(\frac{5}{3}\Theta + \frac{1}{3}\pi)}{3\rho^{5/3}} \right], \end{aligned} \right\} \quad (5.51)$$

where

$$\Theta = \tan^{-1}(\tilde{z}/|\tilde{y}|).$$

An important check on the present analysis is to verify that the above results for large ρ (made dimensionless with length-scale $\delta Re^{1/2} a_0$) match on to those of the previous subsection (where lengths are scaled with respect to a_0). The check is most easily made by comparing the present Fourier transforms (5.49) with those, such as (5.23a), that determine the flow (on length-scale a_0) due to a point sink in the wall of a tube. They can be seen to be exactly the same, with l in (5.49) corresponding to ω in (5.23a), apart from a factor π which arises because the θ -spectrum in § 5.2.2 is discrete, while the \tilde{y} -spectrum here is continuous. The functional forms of τ

and τ_v in (5.51) are somewhat different from the corresponding quantities in (5.27) and (5.28), again because of the inversion in terms of \tilde{y} representing the wall as an unbounded plane, rather than θ representing the bounded geometry of the parent tube.

Despite these differences, however, the main qualitative features of the results are the same. The pressure distribution in (5.50) is the same as the limit of (5.26) as θ and $|s| \rightarrow 0$, apart from the different scaling factor of this subsection and the step rise in pressure represented by the term $H(s)$ in (5.26). This rise is once more a consequence of the inversion in terms of θ , instead of \tilde{y} . The azimuthal shear is also the same: if we let $|\tilde{y}/\tilde{z}| \rightarrow 0$ in (5.51) we see that $\tau_v \rightarrow 0$ upstream ($\Theta = -\frac{1}{2}\pi$) but not downstream ($\Theta = +\frac{1}{2}\pi$) where it decays as $|\tilde{z}|^{-5/3}$ (cf. (5.28)). The downstream decay of τ , on the other hand, is as $|\tilde{z}|^{-2/3}$ in a wake region whose width is zero on this length-scale, but as $|\tilde{z}|^{-5/3}$ outside it, which again agrees with (5.27). The only difference here is that the upstream decay of τ is also as $|\tilde{z}|^{-5/3}$, not purely exponential (i.e. zero) as predicted in (5.27); this too must be a consequence of the unbounded geometry assumed here (since the Fourier transform of τ is the same in each case) and would not be maintained on a length-scale a_0 . More detail about the angular dependence of the wall pressure and shear can be seen from contour plots; single contours for each quantity have been derived from (5.50) and (5.51), and are shown in fig. 5.20. Further information would require numerical inversion of the Fourier transforms (5.44) for $O(1)$ values of \tilde{y} and \tilde{z} , which has not yet been performed (see Brighton (1977) for similar results concerning the flow of a two-dimensional boundary layer over a small three-dimensional hump on the wall). Note from fig. 5.20(b) that the longitudinal component of wall shear is enhanced in regions surrounding the \tilde{z} -axis both upstream and downstream of the hole (as one would predict from a two-dimensional study (Sobey, 1977)), but is diminished in the region $-36^\circ < \Theta < 72^\circ$. Note too that according to these asymptotic results there are, in the wake of the hole, discontinuities both in the \tilde{y} -derivative of the axial component of wall shear (in addition to the singular term in (5.51)) and in the azimuthal shear component itself. No such discontinuities are predicted upstream. A closer examination of the wake region is required to understand this singular behaviour.

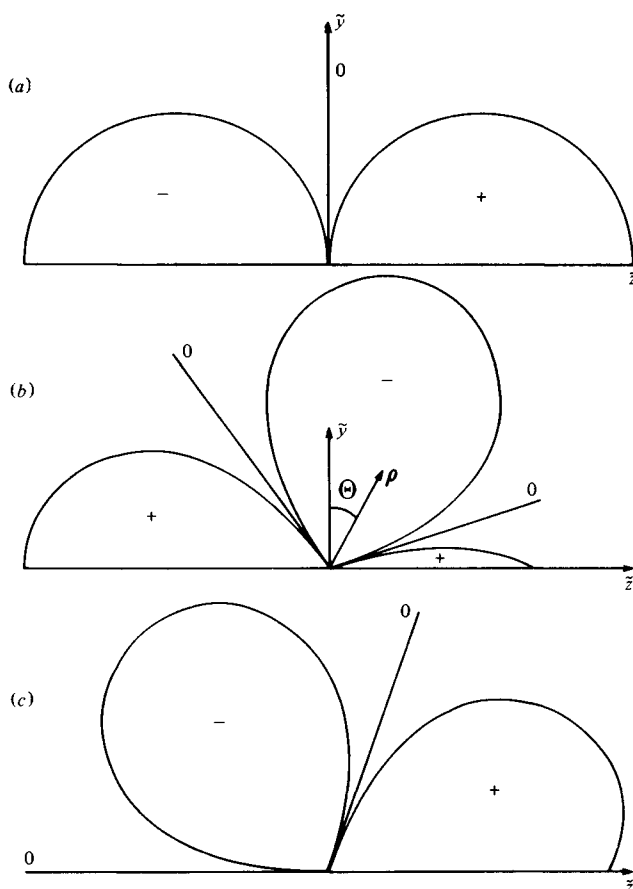


Fig. 5.20. Contour plots of (a) the wall pressure, $p|_{\xi=0}$, (b) the perturbation, τ , to the longitudinal component of wall shear, τ_θ , all derived from the asymptotic results for large ρ ; see (5.50) and (5.51). Regions of the wall in which the plotted quantities are positive and negative are marked accordingly.

Wall pressure and shear far from the hole: $\rho \rightarrow \infty$, $|\tilde{y}| \ll |\tilde{z}|$

In order to examine the wake we must let m become much larger than l as $l \rightarrow 0$. The asymptotic expansions (5.49) remain unchanged as m is increased until $m = O(l^{1/3})$, when $\gamma = O(1)$ and the first two terms of (5.45) become as large as the term involving $[I_+(\gamma) + I_-(\gamma)]$. At this stage the three quantities in (5.44) take the form of powers of l times functions of $(m/l^{1/3})$; the respective powers of l

are

$$\bar{p}|_{\xi=0} \sim l^{1/3}, \quad \bar{\tau}_v \sim l^{1/3}, \quad \bar{\tau} \sim l^{-1/3}.$$

Upon inversion, the additional terms in the three physical quantities themselves can be seen to take the form of powers of \tilde{z} times functions of a similarity variable $\eta = \tilde{y}/\tilde{z}^{1/3}$, as predicted by Jackson (1973): the power of \tilde{z} corresponding to l^ν is $\tilde{z}^{-(4/3+\nu)}$. However, the details of this wake region for $\eta = O(1)$ are complicated and have not been examined in any further detail. Instead, we proceed to examine the innermost part of the wake, keeping $\tilde{y} = O(1)$ as $\tilde{z} \rightarrow \infty$; this requires that in the transformed quantities we keep m (and hence k) equal to $O(1)$ as $l \rightarrow 0$. We therefore require the asymptotic expansions of the integrals arising in \bar{P} , from (5.45), as $|\gamma|$, from (5.41), tends to infinity.

These expansions are derived by deforming the contour of integration in the integrals of both (5.46) and (5.48) to lie along the line

$$\arg \zeta = -\frac{1}{3}\pi \operatorname{sgn} l = \arg \gamma,$$

and then to use the method of stationary phase. The eventual results, when $\arg \xi = -\frac{1}{3}\pi \operatorname{sgn} l$ and $|\xi| \rightarrow \infty$, are

$$\left. \begin{aligned} I_-(\xi) &\sim \frac{\exp \{i \operatorname{sgn} l [\frac{1}{4}\pi + |\xi|^{3/2}(\frac{2}{3} + \delta') - |\gamma|^{1/2}|\xi|]\}}{2\sqrt{\pi}(0 + \frac{1}{2}il)^{1/3}(1 + \delta')|\xi|^{3/4}}, \\ I_+(\xi) &\sim \frac{\exp \{i \operatorname{sgn} l [|\xi|^{3/2}F(\delta') + |\gamma|^{1/2}|\xi|]\}}{2(0 + \frac{1}{2}il)^{1/3}(2 - \delta')^{1/2}} \\ &\quad \times \operatorname{erfc} \left[e^{-i \operatorname{sgn} l \pi/4} \frac{|\xi|^{3/4}(1 - \delta')}{(2 - \delta')^{1/2}} \right], \end{aligned} \right\} \quad (5.52)$$

where

$$\delta' = |\gamma/\xi|^{1/2} \leq 1 \quad \text{and} \quad F(\delta') = \frac{2}{3} - \delta' - (1 - \delta')^2/(2 - \delta').$$

This means that, as $|\gamma| \rightarrow \infty$,

$$I_+(\gamma) \sim \frac{\exp \{i \operatorname{sgn} l \frac{2}{3}|\gamma|^{3/2}\}}{2(0 + \frac{1}{2}il)^{1/3}} \left[1 + \frac{e^{i \operatorname{sgn} l \pi/4}}{6\sqrt{\pi}|\gamma|^{3/4}} \right], \quad (5.53)$$

which is $O(|l|^{-1/3} \exp \dots)$, while

$$I_-(\gamma) = O(|\gamma|^{-3/4}|l|^{-1/3} \exp \dots) = O(|l|^{1/6} \exp \dots)$$

as $|l| \rightarrow 0$ with $|k| = O(1)$. The asymptotic forms for J_\pm can be

evaluated in a similar way, and we finally obtain

$$I \sim -\frac{\exp\{i \operatorname{sgn} l(\frac{1}{4}\pi + \frac{4}{3}|\gamma|^{3/2})\}}{16\sqrt{\pi k}(0 + \frac{1}{2}il)^{2/3}|\gamma|^{3/2}} \left(1 - \frac{e^{i \operatorname{sgn} l \pi/4}}{2\sqrt{\pi}}\right), \quad (5.54)$$

which is $O(|l|^{1/3} \exp \dots)$ as $|l| \rightarrow 0$, so that the term $2\alpha I$ in \bar{P} (see (5.45)) is the same order of magnitude as $I_-(\gamma)$, and smaller than $I_+(\gamma)$. Substitution of (5.52)–(5.54) into (5.44) then gives the following expansions for the Fourier transforms of the perturbation pressure and shear components at the wall:

$$\left. \begin{aligned} \bar{p}|_{\xi=0} &\sim -2k - (il/4k^2)(\frac{25}{6} + 8k^2 K_W), \\ \bar{\tau}_v &\sim im[1 + (il/k)K_W + (0 + \frac{1}{2}il)^{1/2}/2k^{3/2}], \\ \bar{\tau} &\sim il - (2k^2 - m^2)K_W/k + \frac{1}{4}\sqrt{\pi k}^{1/2}/(0 + \frac{1}{2}il)^{1/2}. \end{aligned} \right\} \quad (5.55)$$

If we ignore singularities at the origin these expressions can be inverted to give

$$\left. \begin{aligned} p|_{\xi=0} &\sim 25\tilde{z}/48\pi\rho^2 + 1/\pi\rho^3, \\ \tau_v &\sim 3\tilde{y}\tilde{z}K_W/2\pi\rho^5 + \operatorname{sgn} \tilde{y} H(\tilde{z})/8\pi|\tilde{y}|^{1/2}|\tilde{z}|^{3/2}, \\ \tau &\sim 3\tilde{z}^2 K_W/2\pi\rho^5 - H(\tilde{z})/8\sqrt{\pi}|\tilde{y}|^{3/2}|\tilde{z}|^{1/2}, \end{aligned} \right\} \quad (5.56)$$

where the \tilde{y} - and \tilde{z} -dependence of p and of the first terms in τ_v and τ have been written out in full, but only the small- \tilde{y} limits of the last terms have been given because of the complicated nature of the functions (of \tilde{y}^2/\tilde{z}^2) that arise. Subsequent terms in the expansion of which (5.56) gives the leading terms can be shown to be regular at $\tilde{y} = 0$ for both positive and negative values of \tilde{z} . Indeed, the pressure perturbation given above is everywhere regular (except at the origin) and varies in approximately the same manner as that given by (5.50).

However for $\tilde{z} > 0$ the wall shear distributions, τ_v and τ , contain terms that are singular at $\tilde{y} = 0$, although they can be written respectively as $\tilde{z}^{-5/3}$ and \tilde{z}^{-1} times functions of η , as already predicted. This shows that yet a third distinct region must be considered, at the centre of the downstream wake. In this region there will be a deficit in axial wall shear (the minus sign in the last term of (5.56)) and an outwardly directed flow at the wall itself. This inner wake, or 'corridor', must have lateral length-scale comparable

with the radius, b , of the side-branch, so that $y = O(1)$ ($\tilde{y} = O(\delta Re^{1/2})$), and the details of the motion are presumably dependent on the exact distribution of the flow across the mouth of the side-tube. The present analysis can be used to verify this if the actual distribution of u is used instead of the delta function in (5.38), so that $\bar{u}(\xi = 0)$ is a known function of l and m , say $\bar{u}_0(l, m)$, instead of 1. The only differences in equations (5.44), (5.45) and (5.55) are that $\alpha = (k\bar{u}_0 + i l K_W)/I_-(\gamma)$, and that all terms not involving α or K_W are multiplied by \bar{u}_0 . As an example, suppose that Poiseuille flow enters the mouth of the side-branch:

$$\tilde{u}(0, \tilde{y}, \tilde{z}) = 1 - (\tilde{y}^2 + \tilde{z}^2)/\tilde{b}^2,$$

where $\tilde{b} = \delta Re^{1/2}$ is the dimensionless radius of that branch. Then

$$\bar{u}_0 = J_2(k\tilde{b})/\pi k^2,$$

where J_2 is a Bessel function, and the singular term in, for example, $\bar{\tau}_v$ (see (5.55)) becomes instead

$$im(0 + \frac{1}{2}il)^{1/2} J_2(k\tilde{b})/2\pi k^{7/2}.$$

Inversion shows that, as $\tilde{z} \rightarrow \infty$, this contribution to τ_v is

$$\frac{\tilde{b}^2 \operatorname{sgn} \tilde{y} H(\tilde{z})}{64\pi^2 |\tilde{z}|^{3/2} |\tilde{y}|^{1/2}} F(\frac{3}{4}, \frac{1}{4}; 3; \tilde{b}^2/\tilde{y}^2) \quad \text{for } |\tilde{y}| > \tilde{b}$$

and

$$\frac{\tilde{b}^{1/2} \tilde{y} H(\tilde{z})}{16\pi^{5/2} |\tilde{z}|^{3/2}} \frac{\Gamma(\frac{3}{4})}{\Gamma(\frac{9}{4})} F(\frac{3}{4}, -\frac{5}{4}, \frac{3}{2}; \tilde{y}^2/\tilde{b}^2) \quad \text{for } |\tilde{y}| < \tilde{b},$$

where F is the hypergeometric function (Gradshteyn & Ryzhik, 1965). It can be readily confirmed that these two expressions are equal at $|\tilde{y}| = \tilde{b}$, and nowhere become infinite. Note too that they tend to zero as $\tilde{b} \rightarrow 0$ for all \tilde{y} .

We are thus forced to conclude that however small and weak the side-branch is, there is downstream of it a narrow corridor in which the flow has a different behaviour from that in the $\tilde{y} = O(\tilde{z}^{1/3})$ wake predicted by Jackson (1973). Such corridors have been predicted downstream of somewhat larger perturbations, such as a three-dimensional hump in a two-dimensional boundary layer, when the lateral length-scale of the hump is comparable with the thickness of the boundary layer (Brighton, 1977). However, the conclusion in

this case is more surprising, because one might have expected the effect of lateral diffusion (in the \tilde{y} -direction) to smooth out the detailed influence of the original disturbance over such a small length-scale. That it does not do so must be a consequence of the secondary motions induced by the shear flow past the three-dimensional disturbance, although more research will be needed to understand all the implications of this result. The existence of the corridor adds considerable weight to the above argument (p. 276) that passive mechanical factors may be responsible for the observations of Cornhill & Roach (1976) on the distribution of atheroma downstream of the intercostal arteries in cholesterol-fed rabbits.

Wall pressure and shear near the hole: $\rho \rightarrow 0$

This region can be examined by letting l and m (and hence k) tend to infinity together. In this limit, too, $|\gamma| \rightarrow \infty$, so that (5.55) again gives the required Fourier transforms, and (5.56) again gives the asymptotic form of the quantities of interest, although the singular terms are relevant only when $\tilde{z} > 0$ and $|\tilde{y}/\tilde{z}| \ll 1$, i.e. in the corridor. The important thing to notice about the non-singular terms in the wall shear is that they are exactly the same as those given by (5.36); that is, the small- ρ limit of the present expansion does match with the large- ρ limit of the Stokes flow solution, apart from the existence of the corridor which is, of course, absent when there is no shear flow past the mouth of the side-hole.

5.3 The instability of flow in the aorta

We saw in § 1.2 that blood flow in the aorta of men and horses (and probably other large mammals) appears normally to become turbulent at or shortly after the time of peak aortic velocity. The results shown in fig. 1.26 indicate that turbulence tends to occur if the peak Reynolds number, $\bar{R}e$, exceeds about 250α , where α is Womersley's parameter. In this section we briefly review the possible origins of aortic turbulence.

It is clear from the relative absence of turbulence during the early part of systole and during diastole that the amplitudes of the high-frequency disturbances that constitute the turbulence grow very rapidly just after peak systole, and die away again before the

end of the beat. A detailed spectral analysis by Parker (1977), in terms of wave *number* (frequency divided by instantaneous ensemble-averaged velocity), confirms the observation. This suggests that the growth of the disturbances represents some form of hydrodynamic instability rather than the convection or propagation to the measurement site of fully developed disturbances from upstream. Furthermore, Nerem *et al.* (1972) and Nerem *et al.* (1974a) report that the turbulence is not confined to 'first-beat blood', i.e. to the blood that has been ejected from the ventricle during the beat in which it is observed. Convection of the disturbances known to be present in the left ventricle cannot account for the presence of turbulence in 'second-beat blood'. On the other hand, these authors noted a marked reduction of turbulence intensity with distance down the aorta, which is consistent with the presence of disturbances whose amplitude, albeit growing from a local instability, is proportional to the amplitude existing before growth began. Thus the amplitude in 'first-beat blood' would be expected to be greater than that farther downstream. These observations are inconsistent with an explanation that relies on wave propagation along the vessel walls to transmit the disturbances to the measurement site, since, according to the data presented in § 2.1, that would cause the amplitude to decay too rapidly: the disturbance amplitude decays like $e^{-kx/\lambda}$, where k lies between 0.7 and 1.0 (see p. 78) and an upper limit for the wavelength λ is one tube diameter. Hence the disturbances would lose at least 50% of their amplitude per diameter, a much greater loss than is observed.

Thus the questions to be answered in this section are what mechanisms of instability might be operative in the aorta, and how might they account for the critical peak Reynolds number \hat{Re}_c being approximately 250α . The proportionality of \hat{Re}_c and α can be explained in general terms if the instability mechanism is quasi-steady, i.e. if the unsteadiness of the flow plays only a modulating part in the mechanism (as suggested by the short periods and growth times of the observed disturbances compared with the duration of systole). This follows because if growth of disturbances is possible whenever the local Reynolds number Re exceeds a certain critical value, such as about 2300 for Poiseuille flow in a straight tube, then infinitesimal disturbances will grow to an observable amplitude only

if Re exceeds its critical value for a sufficient length of time. Higher values of α mean a higher frequency and hence a shorter time for Re to exceed its critical value. Therefore, on the assumption that the growth rate of the disturbances increases with Re , it is necessary for the peak Reynolds number \hat{Re} to increase in order for turbulence still to be observed as α increases. This argument is consistent with experimental observations on slowly modulated Poiseuille flow by Sarpkaya (1966).

The most obvious mechanism that can be expected to produce instability just after peak systole is that associated with the appearance of a point of inflection in the velocity profile. In steady parallel flows this is known to cause a strong instability at values of the Reynolds number well below that at which profiles without such an inflection point become unstable. This was the mechanism favoured by Nerem *et al.* (1972), and will be further discussed below. First, however, we consider other mechanisms, associated with vessel-wall elasticity and vessel curvature.

Flow in an elastic tube can cause instability by the mechanism that produces aerodynamic flutter in flow past any elastic wall. That mechanism is essentially the same as Kelvin–Helmholtz instability in which inviscid flow past a plane, indefinitely extensible boundary at rest generates growing waves on that boundary. An elastic boundary resists such deformations, but if the velocity of the flow is great enough there will be instability. Shayo & Ellen (1974) have analysed the stability of inviscid flow through a finite section of an elastic tube of circular cross-section, of length l and undisturbed radius a , joined at each end to a segment of rigid tube also of radius a . The tube wall is taken to be homogeneous, isotropic, linearly elastic and thin, and its deformations are described by Flügge's shell theory. This model is clearly not directly applicable to an artery *in vivo*, but the results should be qualitatively relevant. The analysis shows that instability will occur first for either the 'beam' mode (azimuthal wave number 1) or the 'shell' mode (azimuthal wave number 2) in which the cross-section of the tube becomes elliptical. The 'beam' mode, in which the whole vessel will be displaced sideways at any station, is unlikely to be relevant for a tethered aorta, so we quote results only for the 'shell' mode. Shayo & Ellen (1974) show that the critical velocity U above which instability is

expected is given approximately by

$$U^2 = E\beta^3\omega_n^2/36\rho AQ_n,$$

where

$$\omega_n^2 = (4 + A^2)^2 - (4 + A^2)^{-2}[112 + 100A^2 + (24 - 9/\beta^2)A^4 + A^6],$$

$$Q_n = \frac{A}{8} \left[1 - \frac{1.68A}{n\pi^2} - \frac{A^2}{12} + \frac{0.336A^3}{n\pi^2} + \frac{A^4}{230} \right],$$

$$A = n\pi a/l,$$

and n is the longitudinal wave number. E is the Young's modulus of the wall, ρ is its density, $\beta = h/a$ the thickness-radius ratio, and we have taken the Poisson's ratio to be 0.5. If we choose $E = 5 \times 10^5 \text{ N m}^{-2}$, $\beta = 0.15$, $\rho = 10^3 \text{ kg m}^{-3}$, to represent the aorta, we find that the most unstable mode for $a/l = O(1)$ is $n = 3$, where the critical velocity is about 3.6 m s^{-1} . For longer elastic segments (a/l smaller) or for larger Young's modulus (as in more peripheral arteries), the critical velocity is greater. Thus the predicted critical velocities are significantly greater than those actually present in the aorta, and this is therefore unlikely to be a relevant mechanism of instability. Furthermore, it is hard to see how the buckling of the tube wall in the shell mode can lead to turbulence of the sort observed, except through local flow separation off large-amplitude constrictions, which are not observed. In fact this mode of instability is more relevant to the model experiments reported in chapter 6 and to relatively thin-walled veins than to the observation of turbulence in the aorta.

Curvature of a tube appears to offer the possibility of instability in the form of Taylor-Görtler vortices on the outside wall, where the primary flow is parallel to a surface that is concave in the flow direction. If the flow is assumed to be quasi-steady, quasi-two-dimensional and quasi-parallel to the wall, then instability is predicted to occur if

$$T = (U_\infty \delta_2 / \nu)(\delta_2 / R)^{1/2} \geq T_c, \quad T_c = 0.3, \quad (5.57)$$

where U_∞ is the velocity just outside the boundary layer on the concave wall, R is the radius of curvature of the wall, ν is the kinematic viscosity of the fluid and δ_2 is the momentum thickness of the boundary layer (Schlichting, 1968, p. 506). If the boundary

layer grows gradually in the x -direction, as for the Blasius layer on a flat plate, then transition to turbulence is observed to take place if $T \geq 7$. These results will be relevant to quasi-steady flow near the entrance of a curved tube as long as the developing secondary motions do not affect the stability criterion. In the case of a flat plate, the momentum thickness is given by

$$\delta_2 = 0.664(\nu x / U_\infty)^{1/2},$$

where x is the distance from the leading edge (Schlichting, 1968, p. 131). Combined with (5.57), with $T_c = 7$, this shows that transition to turbulence is predicted if

$$Re \geq 28\,000\delta^{-2}(a/x)^3, \quad (5.58)$$

where Re is based on the tube radius, a , and $\delta = a/R$. Now the theories of §§ 3.2 and 4.4 suggest that the boundary layer thickness does not grow indefinitely with x , being limited both by curvature (in steady flow) and by the Rayleigh layer thickness (in unsteady flow) to a value roughly equal to its value at $x = 5$ cm. In the canine aorta $a = 0.75$ cm and $\delta \approx 0.2$, so (5.58) predicts turbulence if $Re > 2360$, i.e. $U_\infty \geq 1.25$ m s⁻¹. This value of Re is comparable with the critical Reynolds number for flow in a straight tube, and suggests that steady flow in a tube like the aorta might become unstable by either of the two mechanisms. Furthermore, the predicted critical velocity is comparable with the peak measured velocity in the aorta. However, according to (5.58) the flow should become more unstable (i.e. turbulent at a lower Reynolds number) as the curvature δ increases, whereas experiments by White (1929) and Taylor (1929) show that the critical Reynolds number for flow in a curved tube increases markedly as δ increases, which is not consistent with the predictions. While this does not completely rule out the possibility of quasi-steady instability associated with vessel curvature, it does suggest that the neglected secondary motions may have an important stabilising influence that should be examined further.

The above arguments have been based on the assumption of quasi-steady flow. However, Seminara & Hall (1976, 1977) have demonstrated the existence of a mechanism of instability for flow with curved streamlines for which the unsteadiness of the flow is vital. Their theory (and experiment) concerned the flow between

concentric circular cylinders when the outer one is at rest and the inner one (radius a) is rotated with an angular velocity that varies sinusoidally with time with zero mean: $\Omega = (U_0/a) \cos \omega t$ (the corresponding steady motion is that which leads to Taylor vortices). They found that the flow becomes unstable when the Taylor number, $2(U_0\delta_s/\nu)^2(\delta_s/a)$, based on the thickness $\delta_s = \sqrt{(\nu/\omega)}$ of the Stokes layer on the inner cylinder, exceeds a critical value (about 164) and that the instability takes the form of toroidal vortices as in steady flow, except the lateral and longitudinal length-scale of these vortices is δ_s , not the difference in cylinder radii. Seminara & Hall have pointed out that instability by this mechanism might occur near the inside wall of the arch of the aorta, in the same way that Taylor–Görtler vortices might occur on the outside wall. The only factor that would tend to prevent it is the presence of secondary motion. No direct evidence, *in vivo* or in model curved tubes, is yet available.

We revert now to the ‘obvious’ instability mechanism, associated with the point of inflection that is present in the velocity profile during deceleration. The first question to be asked is whether the flow can be regarded as quasi-steady: as remarked above, the high frequency and rapid growth-rate of the observed disturbances, compared with the frequency of the basic flow, suggest that it can. More formally, a time-scale associated with eddies that fill the vessel is a/U , where a is the vessel radius and U the local ensemble-average velocity. This is an upper limit for the disturbance time-scale because most eddies are smaller. This time is short compared with the duration of the decelerative phase (approximately equal to $2\pi/6\omega$, where $\omega/2\pi$ is the heart-rate in Hz) as long as $\omega a/U \ll 1$, i.e. as long as $\alpha^2/Re \ll 1$, where Re is the instantaneous Reynolds number and α is Womersley’s parameter; in the canine aorta, $\omega a/U < 0.1$ if $U \geq 24 \text{ cm s}^{-1}$. The time-scale is also much shorter than the diffusive time-scale a^2/ν as long as $Re \gg 1$, which is clearly satisfied for almost all of systole. Thus the flow in the canine aorta is quasi-steady for much of systole. In a similar problem, that of the stability of the flow in a channel that is suddenly blocked off so that the Poiseuille flow present before the blocking decays away to zero in a time proportional to a^2/ν , Hall & Parker (1976) have confirmed the instability problem to be quasi-steady by using a

WKB expansion. A similar approach could no doubt be followed in this case, although the 'slow' time-scale would have to be chosen to be $2\pi/\omega$ not a^2/ν .

Given that the problem is quasi-steady, let us consider what happens as the velocity profile evolves from its inflection-free state at peak systole. Immediately deceleration begins, an inflection point appears near the wall. According to inviscid stability theory this would be unstable for disturbances whose wavelengths were greater than a certain critical value. However, viscous theory would show that, if the inflection point were weak enough (i.e. if d^3U/dr^3 were sufficiently small) or if it were close enough to the tube wall, disturbances could not grow. At some time after peak systole, however, the flow would become unstable to disturbances of a particular wavelength which would start to grow. A little later still, the flow would be unstable to disturbances of other wavelengths, and the most rapidly growing disturbance may not be that which first became unstable. Thus in order to predict the first disturbance to become large enough to be seen one would have to study the (linear) evolution of all disturbances, while the basic flow varied slowly, and see which first reached a certain critical amplitude (cf. Gaster (1974), on the instability of spatially varying flows). However, unstable disturbances in parallel flows rapidly become non-linear, and a catastrophic transition to turbulence takes place, so the best that can be hoped for from linear theory is a prediction of when instability first occurs and when disturbances should first be observable, involving a prediction of the growth-rates and wavelengths of the most rapidly growing disturbances. (See Davis (1976) for a broader discussion of the instability of periodic flows.)

Until some recent work by Dr A. J. Sobey (personal communication; see below), such predictions had not, as far as I know, been made for time-dependent flow in a straight circular-cross-section tube, because the corresponding steady, linear instability problem had not been solved for the family of velocity profiles involved. The only previous computations I am aware of on the instability of velocity profiles with inflection points in viscous fluids are those by Obremski, Morkovin & Landahl (1969) for the Falkner-Skan boundary layer on a wedge with a slight adverse pressure gradient, by Eagles & Weissman (1975) for flow in a

slightly divergent channel, and by Hall & Parker (1976) on the decaying flow in a blocked channel. The first study considered only steady quasi-parallel flows, the second was a complete study on steady flows with slow *spatial* variation, and the last, although concerned with a temporally slowly varying basic flow (calculated by Weinbaum & Parker, 1975), did not compute the evolution of unstable disturbances when the Reynolds number is large, but concentrated instead on the properties of the neutral disturbances at different times and Reynolds numbers. Hall & Parker's results (and some experiments by K. H. Parker, personal communication) confirm that the inflection point causes instability at a much lower Reynolds number than the critical value for plane Poiseuille flow. If the channel width is $2h$ and the maximum velocity of the Poiseuille flow is U_0 , then the critical Reynolds number $U_0 h / \nu$ before the channel is blocked is 5750 (Grosch & Salwen, 1968), while afterwards it is about 150. Instability first occurs at a time $0.023 \nu / h^2$ after blocking of the flow; if ν is the kinematic viscosity of blood and h the radius of the aorta, this time is about 1.6 ms. Because Hall & Parker's flow is stopped more suddenly than that in the aorta, their estimate of the time to instability (at $Re \approx 150$) is likely to be an underestimate, although it will, of course, be an overestimate of the time to instability of a suddenly stopped flow at higher values of Re . In any case, the time is so short that there is clearly plenty of time for such an instability to grow in the aorta.

Nerem *et al.* (1972) made a comparison of their results with the theory of Obremski *et al.* (1969). Fig. 5.21 shows plots of dimensionless wave number against Reynolds number, each based on the displacement thickness δ_1 of the boundary layer under consideration. The curves are the theoretical neutral curves computed by Obremski *et al.* for different values of the Falkner–Skan parameter β ($= 2n/n + 1$, where the velocity outside the boundary layer is proportional to x^n). The points are experimental ones for which the boundary layer displacement thickness was calculated from the solution for the Rayleigh layer (see (3.33)) and the wave number was chosen to be that associated with disturbances at a frequency of 125 Hz, representative of measured frequencies. This figure is consistent with the idea that the point of inflection is important for instability, since all points lie outside the unstable region for $\beta = 0$,

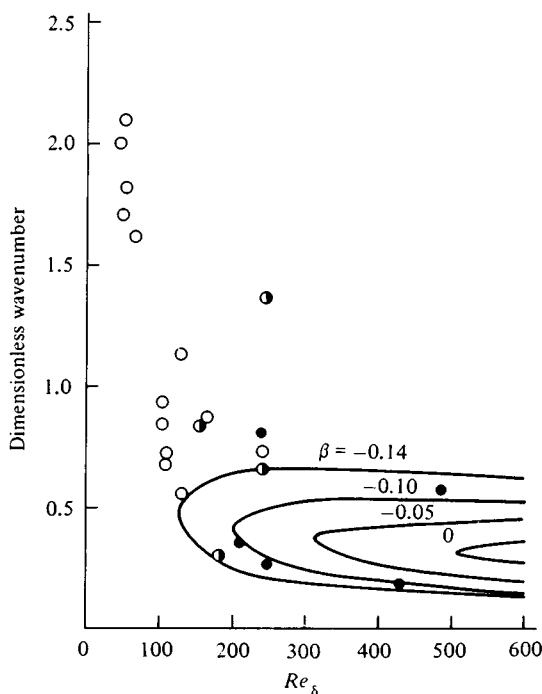


Fig. 5.21. Comparison of experimental observations with Falkner-Skan neutral stability curves from Obremski *et al.* (1969): undisturbed flow, open circles; disturbed flow, half-filled circles; highly disturbed flow, full circles. (After Nerem *et al.*, 1972.)

while many of the disturbed or turbulent points lie inside the unstable region for β between -0.10 and -0.14 . More quantitative conclusions could not be made, since further progress requires computations of the sort recommended above.

Nerem *et al.* also gave an extremely crude theoretical argument for the proportionality between the critical peak Reynolds number \hat{Re}_c and α . Steady boundary layer instability theory, with or without an adverse pressure gradient, shows that boundary layers become unstable if the Reynolds number based on boundary layer displacement thickness δ_1 exceeds a critical value:

$$U\delta_1/\nu > Re_{\delta c}.$$

But in unsteady periodic flows $\delta_1 = k(\nu/\omega)^{1/2}$ for some constant k ,

so instability is predicted if $U(\omega\nu)^{-1/2}$ exceeds $Re_{\delta c}$, i.e. if

$$Re > \alpha Re_{\delta c}/k.$$

This is the required result. Note that for a sinusoidal oscillation, $k \approx 1$, while for a Falkner–Skan flow with $\beta = -0.10$, $Re_{\delta c} \approx 200$ (fig. 5.21). Hence $Re_{\delta c}/k \approx 200$, which is not far from the observed value of about 250.

Some more detailed computations on flow in a straight circular-cross-section tube have now been made by Dr A. J. Sobey at Imperial College, London (personal communication). He chose an undisturbed velocity profile consisting of a mean Poiseuille flow plus a component corresponding to a single sinusoidal oscillation in pressure gradient of frequency ω (c.f. (2.34) or (3.1)). He restricted attention to quasi-steady disturbances (i.e. $Re \gg \alpha^2$ and $Re \gg 1$, see p. 296), and performed numerical integration of the Orr–Sommerfeld equations for various values of the three remaining dimensionless parameters: α , γ (the ratio of the pressure-gradient amplitude to its mean), and T ($= (\bar{Re}/\alpha^2)\omega\hat{t}$) which represents the time within the cycle. At the time of writing not many results were available, but one example that has been calculated is that for which $\alpha = 10$ and γ is chosen so that the centre-line velocity just comes to rest each beat. Then instability is first predicted very shortly after the time of peak centre-line velocity (when deceleration begins and an inflection point first appears), and at that time the Reynolds number based on boundary layer displacement thickness, Re_{δ} , is approximately 175. Considering that some time must elapse, and the boundary layer become thicker, before the instability is observed, this too is consistent with the in-vivo value of 250 quoted by Nerem *et al.* (1972).